Insights into lactic acid bacteria cryoresistance using FTIR micro-spectroscopy

Amélie Girardeau, Stephanie Passot, Julie Meneghel, Stéphanie Cenard, Pascale Lieben, Ioan-Cristian Trelea, Fernanda Fonseca

Insights into lactic acid bacteria cryoresistance using FTIR micro-spectroscopy

Amelie Girardeau, Stephanie Passot, Julie Meneghel, Stephanie Cenard, Pascale Lieben

Ioan-Cristian Trelea, Fernanda Fonseca,*

Université Paris-Saclay, INRAE, AgroParisTech, UMR SayFood, 78850, Thiverval-Grignon, France

*****Correspondance email: fernanda.fonseca@inrae.fr

ORCID numbers:

Amélie Girardeau: 0000-0003-3871-5119

Stéphanie Passot: 0000-0003-2799-5493

Julie Meneghel: 0000-0002-1510-8642

Stéphanie Cenard: 0000-0001-5996-1576

Pascale Lieben: 0000-0002-7450-0230

Ioan-Cristian Trelea: 0000-0001-6727-0716

Fernanda Fonseca: 0000-0003-3394-182X

Abstract

Freezing is widely used for bacterial cell preservation. However, resistance to freezing can greatly vary depending on bacterial species or growth conditions. Our study aims at identifying cellular markers of cryoresistance based on the comparison of three lactic acid bacteria (LAB) exhibiting different tolerance to freezing: *Carnobacterium maltaromaticum* CNCM I-3298, *Lactobacillus delbrueckii* subsp. *bulgaricus* ATCC 11842, and *Lactobacillus delbrueckii* subsp. *bulgaricus* CFL1.

A thorough characterization of their cytoplasmic membrane properties was carried out by measuring their fatty acid composition, membrane fluidity, and lipid phase transition upon cooling from 50 °C to -50 °C. Vitrification temperatures of the intra- and extra-cellular compartments were also quantified by differential scanning calorimetry. Additionally, the cell biochemical characterization was carried out using a recently developed Fourier transform infrared (FTIR) micro-spectroscopic approach allowing the analysis of live bacteria in an aqueous environment.

The multivariate analysis of the FTIR spectra of fresh and thawed cells enabled the discrimination of the three bacteria according to their lipid, protein, and cell wall peptidoglycan components. It also revealed freezing-induced modifications of these three cellular components and an increase in bacteria heterogeneity for the two strains of *L. bulgaricus*, the freeze-sensitive bacteria. No cellular damage was observed for *C. maltaromaticum*, the freeze-resistant bacteria. Comparison of the results obtained from the different analytical methods confirmed previously reported cryoresistance markers and suggested new ones, such as changes in the absorbance of specific infrared spectral bands. FTIR microspectroscopy could be used as a rapid and non-invasive technique to evaluate the freeze-sensitivity of LAB.

Keywords: Lactic acid bacteria – Freezing – Membrane properties – Infrared spectroscopy – cryoresistance markers

Introduction

Lactic acid bacteria (LAB) concentrates are widely used today in the food industry to produce various fermented products such as yoghurt, cheese, or kimchi, as well as in the health industry to produce probiotics. Freezing is one of the most employed LAB preservation techniques and a critical step in the production of LAB concentrates. It is nonetheless a stressful stabilization process that can lead to cell damage and death.

During freezing, LAB cells are mainly exposed to cold and osmotic stresses, leading to lipid membrane rigidification, cell dehydration, and volume reduction [1,2]. The cell dehydration and volume reduction induced by the cryoconcentration of the extracellular medium bring about mechanical constraints on the cell membrane and lead to permanent deformation and loss of membrane integrity [3–5]. Furthermore, protein damage induced by freezing has been reported [6]. The cellular freezing-induced damage can be influenced by the addition of protective additives [7–9], as well as cooling, thawing, and storage protocols [10,11].

Cryoresistance of LAB can be increased by inducing active cell responses to cold and osmotic stresses when cells are exposed to changes in culture conditions during fermentation (temperature, pH, nutrients) (see **ESM Table S1**) [12]. Cryoresistance varies also depending on bacterial species or strain [10,13]. Several studies, reported in **Table S1**, have investigated the modifications of cellular components that have been related to an increase of the bacterial survival rate following freezing or frozen storage. The analytical methods applied for characterizing those components are also listed in **Table S1**.

More than 70 % of the reported studies focused on the role of the cytoplasmic membrane on LAB cryoresistance and evidenced the key role of its fatty acid composition. In most works, an improvement of cell viability or acidifying activity after freezing was related to an increase in the ratio between unsaturated fatty acids (UFA) and saturated fatty acids (SFA) [2,5,13–17], and/or an increase in the cyclic fatty acids (CFA) content of the membrane [5,13,15–18]. However, the effect of CFA on LAB cryoresistance remains unclear, since few authors have associated better cryoresistance with a reduction in CFA contents [3,13]. Three studies that deeper investigated the membrane properties of *L. bulgaricus* CFL1 and ATCC 11842, related the increase of the UFA/SFA ratio to a decrease of lipid membrane phase transition temperature (Ts) following cooling (Ts from 14 / 22 °C to -6 / -8 °C measured by FTIR spectroscopy) and to an increase of membrane fluidity at 0 C° (determined by fluorescence anisotropy) [2,5,19]. Consequently, when approaching ice nucleation, the membrane of freeze-resistant cells is in a more fluid and flexible state than the membrane of freeze-sensitive cells and thus better withstands the mechanical constraints following water escape from the cell and the resulting cell shrinkage caused by ice nucleation and ice crystals growth.

However, minor modifications of the membrane fatty acids composition were observed in few studies [20–22], indicating that other cellular components and mechanisms are involved in LAB cryoresistance. Studies investigating the proteome of cryoresistant versus cryosensitive LAB populations, have also linked improved resistance to changes in protein synthesis [21,23–25], and more specifically to the production of cold-shock proteins [23,24]. These proteins are believed to improve cryoresistance by maintaining efficient transcription and translation under low positive temperatures [24,26,27].

In more recent years, FTIR micro-spectroscopy has emerged as a powerful tool to assess biochemical changes in microorganisms caused by stress conditions [6,28–32]. A study investigating the FTIR spectral features of dried samples of two *L. bulgaricus* CFL1 populations presenting different cryoresistance levels, revealed potential markers of cryoresistance related to cellular lipids, protein secondary structures, and cell wall components [6]. To avoid potential bias induced by sample drying, Meneghel et al. [33], developed an FTIR micro-spectroscopic approach enabling the accurate exploitation of the entire mid-infrared region of bacterial cells in aqueous conditions. This was achieved using a custom-built sample chamber and a specifically developed water subtraction program, able to greatly reduce the spectral contribution of water.

In this study, we aimed to complete the work of Meneghel et al. [2,33] by applying the developed FTIR approach to obtain the biochemical composition of fresh and thawed samples of *L. bulgaricus* ATCC 11842, *L. bulgaricus* CFL1and *C. maltaromaticum* CNCM I-3298. The latter was included in this research because it is an extremely cryoresistant LAB reported to present no viability loss after 11 freeze-thaw cycles [34]. Moreover, *C. maltaromaticum* was shown to maintain its cryoresistance despite changes in growth conditions (temperature, pH, and harvest time) [35]. The membrane fatty acid composition, lipid membrane phase transition following freezing, membrane fluidity following cooling, and intracellular glass transition temperature were also measured to extend the range of markers of cryoresistance.

Materials and Methods

The experimental approach and various methods used are shown in **Figure 1**. Unless otherwise indicated, all measurements were performed on three independent bacterial cultures, for each strain. For the experimental methods followed by asterisks in Figure 1, the corresponding data for *L. bulgaricus* strains were taken from Meneghel et al. [2,33].

All the data generated and/or analysed during the current study are available in the Data INRAE repository https://data.inrae.fr/privateurl.xhtml?token=c30d001f-a7d7-4411-8d36-c55bb5968f04.

Bacterial strains, growth conditions, freezing and thawing protocols

Three strains of lactic acid bacteria were used in this study: *Carnobacterium maltaromaticum* CNCM I-3298 (Pasteur Institute, Paris, France), *Lactobacillus delbrueckii* subsp. *bulgaricus* CFL1 (CIRM-BIA; Rennes, France) and *Lactobacillus delbrueckii* subsp. *bulgaricus* ATCC 11842 (Manassas, VA, USA).

The *C. maltaromaticum* strain was cultivated and frozen according to the procedure described by Girardeau et al. [35], and the *L. bulgaricus* strains, according to the procedures described by Meneghel et al. [2]. After centrifugation (**Fig. 1**), cell pellets of *C. maltaromaticum* and *L. bulgaricus* were re-suspended in a trehalose solution (20 % wt in saline water) at a weight ratio of 1:2 (1 g of cell pellet and 2 g of cryoprotective solution), or in a sucrose solution (20 % wt in saline water) at a weight ratio of 1:1, respectively. All cryopreserved bacterial concentrates were stored a minimum of 24 h at -80 °C. Thawing was carried out using a water bath set to 30 °C for *C. maltaromaticum* and 42 °C for the *L. bulgaricus* strains. Several freeze-thaw cycles were applied to better assess differences in biological activity recovery.

To determine a potential effect of the protective conditions applied that differed between *L bulgaricus* [2] and *C. maltaromaticum* [35], the biological activity recovery of *C. maltaromaticum* was also investigated for cell pellets re-suspended in a sucrose solution (20 % wt in saline water) at a weight ratio of 1:2 and 1:1 (cell pellet weight: protective solution weight).

Biological activity assessment of cell samples

Culturability

Cell viability was measured using the agar plate count method. Fresh or thawed cell suspensions were diluted in saline water, then plated into an agar growth medium: Plate Count Agar (Biokar Diagnostics, Paris, France) for *C. maltaromaticum* and MRS Agar (Biokar Diagnostics, Paris, France) for the *L. bulgaricus* strains. Incubation was carried out at the strain's respective optimal temperatures for growth

(30 °C for *C. maltaromaticum* and 42 °C for *L. bulgaricus*), for 48 h. The cell plate counts were expressed in CFU.mL^{-1} and results were obtained in triplicate.

Culturability loss after each freezing cycle (FC) (in log[CFU.mL^{-1}]) was calculated using the following equation (Eq. 1):

$$Culturability\ loss\ after\ the\ FC(i) = \log \frac{[CFU\ mL^{-1}]_{thawed\ cells\ after\ FC(i)}}{[CFU\ mL^{-1}]_{thawed\ cells\ after\ FC(i-1)}} \quad \text{(Eq. 1)}$$

For the first freezing cycle (i=1), $[CFU.mL^{-1}]_{\text{thawed cells after FC(i-1)}}$ corresponds to the cell concentration in the fresh sample.

Acidifying activity

Acidifying activity measurements were carried out using the Cinac system (AMS; Frepillon, France) according to the procedure described by Girardeau et al. [35] for *C. maltaromaticum* cells and according to Meneghel et al. [2] for the *L. bulgaricus* cells. Briefly, flasks containing 150 mL of sterile culture medium were pre-warmed to the optimal temperature for growth of each of the studied strains. Following the inoculation of a flask with a precise volume of cryoprotected bacterial suspension (15 µL for *C. maltaromaticum* suspensions or 100 µL for *L. bulgaricus* suspensions), their pH was continuously monitored every 3 min until the end of acidification. Measurements were obtained in triplicate. The minimum of the first-order derivative of the acidifying curves represents the time required for the bacterial suspension to reach its maximum acidifying rate and was used as a discriminating descriptor between fresh and thawed cells within each strain (tm, in min). The higher the tm value was, the lower the acidifying activity was.

Acidifying activity (AA) loss after each freezing cycle (FC) (in min) was quantified as follows:

$$AA\ loss\ after\ FC(i) = tm_{thawed\ cells\ after\ FC(i)} - tm_{thawed\ cells\ after\ FC(i-1)} \quad \text{(Eq. 2)}$$

For the first freezing cycle (i=1), $tm_{\text{thawed cells after FC(i-1)}}$ corresponds to the tm value of the fresh sample.

Characterization of the cytoplasmic membrane

Membrane lipid extraction and gas chromatography: fatty acid (FA) composition

Membrane fatty acid (FA) composition of *C. maltaromaticum* was determined on the cell pellets of thawed, washed bacterial samples, according to the method detailed by Meneghel et al. [2]. Briefly, lipid extraction was performed using an accelerated solvent extractor (ASE 350, Dionex; Sunnyvale, CA, USA), using a chloroform/methanol-based extraction method. The obtained lipids were then mixed with a C9:0 internal standard (Sigma-Aldrich; St. Louis, MO, USA) and methylated using trimethylsulfonium hydroxide (TMSH, Sigma-Aldrich; St. Louis, MO, USA). FA identification and quantification was carried out on a Hewlett-Packard 6890 gas chromatograph (GMI; Ramsey, MI, USA) coupled to a mass spectrometer (5973, Agilent Technologies; Avondale, PA, USA). Results were expressed as relative FA percentages.

Fatty acid compositions of the *L. bulgaricus* strains were recalculated from raw data available from Meneghel et al. [2].

Steady-state fluorescence anisotropy: membrane fluidity

Membrane fluidity of *C. maltaromaticum* was assessed by steady-state fluorescence anisotropy, using a 1,6-diphenyl-1,3,5-hexatriene (DPH) fluorescent probe. The method described by Meneghel et al. [2], with minor modifications, was applied. Stock solutions of DPH (6 mM, Sigma-Aldrich; St. Louis, MO, USA) were prepared in dimethylsulfoxide (DMSO, Sigma-Aldrich; St. Louis, MO, USA).

Briefly, 50 µL of cryoprotected bacterial sample were washed three times in MES –KOH buffer (50 mM, pH 5.5) supplemented with 10 mM glucose. The bacterial pellets obtained after three washes were diluted in 1mL of the same buffer to reach approximately 10^7 cells.mL^{-1}. Ten µL of DPH 6 mM, were added to 1 mL of cell suspension. Just before use, DPH solution was sonicated for 10 min at 20 Hz. After addition of the dye, the cell suspension was vortexed for 1 min, and incubated 3 min in darkness at 30 °C before centrifugation (14,000 × g for 90 sec). The pellet was re-suspended in 3 mL of a 25 % (w/w) of sucrose solution and loaded into a stirred quartz cuvette.

Steady-state fluorescence anisotropy (r) of *C. maltaromaticum* cells were measured in a photoluminescence spectrometer (FLS1000, Edinburgh Instruments, Serlabo Technologies, France). The excitation and emission wavelengths were respectively set at 360 and 430 nm. Polarizers were located on the excitation source and on the photomultiplier tube to measure anisotropy.

Anisotropy values were obtained at different sample temperatures ranging from 42 °C to 0 °C using a Peltier-based temperature-controlled cuvette holder (LFI-3751, Wavelength electronics; Bozeman, MT, USA and Luma 40, Quantum Northwest, WA, USA). Since the anisotropy values of *L. bulgaricus* strains (taken from Meneghel et al. [2]) were obtained on a different equipment (Fluorolog-3 spectrofluorometer, Jobin-Yvon Horiba), a control measurement was carried out on each *L. bulgaricus*

strain using the same equipment and protocol than those used for *C. maltaromaticum*. The results were similar regardless of the equipment used.

FTIR spectroscopy measurements: membrane lipid phase transition

The membrane lipid phase transition of cells during freezing was studied using FTIR spectroscopy, by measuring the position of the symmetric CH_2 stretching vibration band (ν_sCH_2) located around 2850 cm^{-1} and arising from the lipid acyl chains of the cytoplasmic membrane,. The peak position and shape of the O-H libration and bending combination band of water (νH_2O) located around 2200 cm^{-1} was simultaneously monitored to determine ice nucleation temperatures (Tn).

Measurements were carried out on a Nicolet Magna 750 FTIR spectrometer (Thermo Fisher Scientific; Madison, WI, USA) equipped with a variable temperature stage (Specac Ltd.; Orpington, Kent, UK), as described by Meneghel et al. [2]. The optical bench was continuously purged with dry air (Balston; Haverhill, MA, USA) to remove the spectral contribution of water vapor.

Concentrated and protected bacterial samples of *C. maltaromaticum* were washed two times in saline water, re-suspended in a 25 % (w/w) sucrose solution for 15 min at room temperature, before being centrifuged at 16,100 × g for 5 min, according to the preparation applied by Meneghel et al. [2] for the *L. bulgaricus* samples. A small amount of the resulting cell pellet was tightly sandwiched between two calcium fluoride (CaF_2) windows (ISP Optics; Riga, Latvia). Temperature was decreased from 50 °C to -50 °C at a rate of 2 °C.min^{-1} by pouring liquid nitrogen into the cell holder. An accurately controlled cooling rate was insured by a thermocouple inserted as close as possible to the sample. Spectra acquisition was performed throughout cooling by the Omnic software (version 7.1, Thermo Fisher Scientific; Madison, WI, USA): 32 co-added scans were collected in the mid-IR region between 4000 and 900 cm^{-1}, every 45 s at a 4 cm^{-1} resolution. The lipid phase transition (Ts) values of the *L. bulgaricus* strains were taken from Meneghel et al. [2], and their ν_sCH_2 values at the frozen state (-48°C) were obtained from the corresponding raw data.

Spectra analyses were performed using the ASpIR software (Infrared Spectra Acquisition and Processing, INRAE; Thiverval-Grignon, France): the peak positions of ν_sCH_2 and νH_2O in each spectrum were determined using their second-order derivatives. Second order derivatives were calculated and smoothed according to a seven-point Savitsky-Golay algorithm. The obtained peak frequencies were then plotted against the temperature at which they were measured.

The ν_sCH_2 plots arising from the *L. bulgaricus* samples were fitted with a curve based on an asymmetric sigmoid transition function and the first derivative was calculated. The maximum of the first derivative of the fitted curves was taken as the lipid membrane phase transition temperature (Ts, lipid solidification following freezing, in °C). In the case of *C. maltaromaticum* samples, plots were fitted with a curve

based on a continuous piecewise function: a linear function for temperatures above Ts and a sum of linear and exponential functions for temperatures below Ts.

DSC measurements: intracellular glass transition temperature

The intracellular glass transition temperature (Tg'i, °C) was determined by differential scanning calorimetry DSC) as described previously [1,2,36]. A power compensation calorimeter (Diamond, Perkin Elmer LLC, Norwalk, CT, USA), equipped with a liquid nitrogen cooling accessory (CryoFill, Perkin Elmer) was used. Cell pellets of *C. maltaromaticum* obtained after harvest were washed three times with peptone water (1 $g.L^{-1}$). About 20–50 mg of a washed cell pellet obtained by centrifugation (14,000 × g for 3 min) was scanned following cooling to -100°C and heating to 20°C at 10 $°C.min^{-1}$ with an acquisition rate of 5 points per second (Pyris software 13.1, Perkin Elmer). Cell concentrations were typically 10^8–10^{10} cells per mL. An empty pan was used as a reference. Temperature calibration was performed using cyclohexane (crystal-crystal transition at −87.1 °C) and mercury (melting point at −38.6 °C).

Additionally, the washed cell pellet with peptone water was resuspended in a sucrose cryoprotective solution (20 % in saline water), incubated for 30 min and then centrifuged. The resulting sucrose protected *C. maltaromaticum* pellet was also analysed to enable the comparison with *L. bulgaricus* results [2].

The first derivative of the heat flow curve recorded during the warming step was calculated and smoothed (50 points smoothing). The glass transition temperature of the intracellular content (Tg'i) was calculated as the maximal value of the peak observed in the first derivative curve. The values of intracellular temperatures of the *L. bulgaricus* strains as well as the value of the extracellular glass transition temperature (Tg'e, °C) (protective sucrose solution) were taken from Meneghel et al. [2].

FTIR micro-spectroscopy: biochemical characterization of cells before freezing and after freeze-thawing, in aqueous conditions

The biochemical characteristics of *C. maltaromaticum* samples in aqueous environment were measured using a FTIR microscope (Nicolet iN10, Thermo Fisher Scientific, Madison, WI, USA), with a permanently aligned objective (15× and 0.7 NA) Liquid nitrogen cooled Mercury-Cadmium-Telluride (MCT) detector and a high resolution 1/3 inch color digital camera (USB2 with 1024 × 768 XGA low-noise CCD). The set up includes a demountable micro-chamber of CaF_2 windows (Hellma Analytics, Paris, France), according to the method recently published and described in more detail by Meneghel et al. [33]

Briefly: fresh and thawed cryoprotected cell suspensions were washed three times in saline water, then centrifuged at 16,100 × g for 5 min. A very small amount (less than one microliter, or the tip of a 200 µL pipette cone) of the resulting pellet was deposited on one side of the micro-chamber, separated from the diluent side (containing saline water) by a 2.5 µm thick strip of Mylar® film (Goodfellow; Lille, France).

Spectra acquisition was performed using the Omnic software (version 8.1; Thermo Fisher Scientific; Madison, WI, USA) with apertures set at 50 x 50 µm. A background spectrum was acquired in an air bubble on the diluent side of the micro-chamber and spectra on multiple areas of both the diluent and the cell sample were measured. Each spectrum was obtained from 128 co-added scans in the mid-IR region between 4000 and 900 cm^{-1} at a 4 cm^{-1} resolution (acquisition time = 45 seconds). The spectra of the *L. bulgaricus* strains were acquired during the PhD project of Julie Meneghel and results obtained from fresh samples were previously published [33].

Spectral pre-processing (see **ESM Fig. S1a** and **Fig. S1b**) was carried out according to the procedure described by Meneghel et al. [33]. No baseline correction was applied in this step. The Omnic software was used for automatic atmospheric correction and spectra sorting. A specifically developed program implemented in Matlab (TheMathWorks Inc., Natick, MA, version 2014a, 8.3.0.532) was applied for water subtraction guided by the method developed by Vaccari et al [37]. This program involves removing an optimized scaled diluent spectrum (average of ten diluent spectra) to the sample spectra. The scaling factor is determined by an algorithm designed to obtain spectra presenting a similar Amide I/II area ratio to those of dried cells. The Amide I/II area ratios of strains in the dry state were 2.17 for *L. bulgaricus* CFL1, 2.34 for *L. bulgaricus* ATCC 11842 (Meneghel et al. [33]) and 2.33 for *Carnobacterium maltaromaticum* CNCM I-3298 (this work). ~~A more detailed description of this water subtraction procedure is presented in Meneghel et al. [33].~~

Post-processing of the water subtracted spectra was done using the Unscrambler® X software package (version 10.2, Camo Software AS; Olso, Norway). In total, 188, 199 and 188 water-subtracted infra-red spectra of fresh and thawed cells from three biological replicates (about 30 spectra for each replicate) were analyzed for *C. maltaromaticum* CNCM I-3298, *L. bulgaricus* ATCC 11842 and *L. bulgaricus* CFL1 cells, respectively.

Analyses were carried out on three main distinct spectral regions (see **ESM Fig. S1**): (i) the 3016 – 2800 cm^{-1} region containing information on fatty acyl chains of the bacterial membrane; (ii) the 1800 – 1370 cm^{-1} region notably containing the Amide I and II bands, the most prominent vibrational bands of the cell proteins backbone; (iii) the 1370 – 975 cm^{-1} region, containing information on protein, nucleic acids and cell wall components (phosphorylated molecules and polysaccharides). A sub-region of (iii), the 1200 – 1000 cm^{-1} region containing information on cell wall components and nucleic acids (PO_2^- groups

and sugar rings) was also analysed. Baseline correction and normalization were performed in each region using an extended multiplicative scatter correction (EMSC) procedure [38].

Resulting spectra were then analyzed by Principal Component Analysis (PCA), to reveal data variance (score plots) and peak positions of interest (loading plots). In the PCA analysis we applied the Non-linear Iterative Partial Least Squares algorithm (NIPALS). The assignment of principal absorption bands was done using data from literature (see **ESM Table S2**).

To confirm spectral bands evidenced by the loading plots in the 1800 – 1370 cm^{-1} and 1200 – 1000 cm^{-1} regions, the ~~normalized and~~ averaged spectra of the three lactic acid bacteria before and after freeze-thawing were calculated (after spectra baseline correction and normalization), and the second-order derivatives were processed using a Savitzky-Golay algorithm (third-degree polynomial and a 9-point smoothing factor).

To visualize the components of the Amide I band (1700 – 1600 cm^{-1}) that provide information on the secondary structure of proteins: α-helix and β-sheet bands, respectively found at ~1654 and ~1637 cm^{-1}, normalization and baseline corrections were performed in the Amide I region (1700 – 1600 cm^{-1}) using an extended multiplicative scatter correction (EMSC. Then, the second derivatives of the spectra were calculated using a Savitzky-Golay algorithm (third-degree polynomial and a 9-point smoothing factor). The height ratios between the α-helix band peak at approximately 1654 cm^{-1} (I_{1654}) and the β-sheet band peak at approximately 1637 cm^{-1} (I_{1637}) in the second derivative spectra ($I_{1654}/1_{1637}$) were calculated and used as a measure for secondary protein structure changes between fresh and thawed cells.

Statistical analysis

The nonparametric Kruskal-Wallis and the post-hoc Conover Iman tests were performed using XLSTAT 19.6 (Addinsoft, Paris, France), to compare data concerning biological activity, fatty acid composition, fluorescence anisotropy, dynamic FTIR spectroscopy, DSC measurements, and $I_{1654}/1_{1638}$ ratio. A significance level of 95 % ($p < 0.05$) was considered.

Results

Cultivability and acidifying activity losses in response to freezing

The loss in culturability and acidifying activity of all three strains after a first and a second freeze-thaw cycle is presented in **Figure 2**. Results for up to seven freeze-thaw cycles are reported in supplementary material (see **ESM Table S3)**.

The highest losses in both culturability and acidifying activity after the first freeze-thaw cycle was measured in *L. bulgaricus* CFL1 (CFL1): -1.46 log units in culturability and +261 min (4.35 h) in acidifying time. *L. bulgaricus* ATCC 11842 (ATCC) showed no significant loss of culturability after the first or the second freeze-thaw cycles, similarly to *C. maltaromaticum* (CM). However, *L. bulgaricus* ATCC 11842 did show loss of acidifying activity after both the first (+23 min) and the second (+15 min) freeze-thaw cycles, while *C. maltaromaticum* did not. After 4 freezing cycles, the cumulative losses in culturability and in acidifying activity for the three strains were the following: 3 log units and 366 min for *L. bulgaricus* CFL1; 0.6 log units and 94 min for *L. bulgaricus* ATCC 11842; and 0 log unit and 14 min for *C. maltaromaticum*. *C. maltaromaticum* showed no significant loss of culturability or acidifying activity for up to 7 freeze-thaw cycles (see **ESM Table S3**), thus confirming *C. maltaromaticum* CNCM I-3298's exceptional cryoresistance.

Among the three studied strains, *C. maltaromaticum* therefore presented the highest cryoresistance, *L. bulgaricus* CFL1, the lowest cryoresistance and *L. bulgaricus* ATCC 11842 intermediate cryoresistance.

The cultivability and acidifying activity losses of *C. maltaromaticum* cells presented above were initially measured in cells frozen in a trehalose-based cryoprotective solution (20 % (wt/wt) in saline water) at a ratio of 1:2, while the *L. bulgaricus* cells were cryoprotected in a sucrose-based solution (20 % (wt/wt) in saline water) at a ratio of 1:1. The cryoresistance of *C. maltaromaticum* cells frozen in a sucrose-based (20 % (wt/wt) in saline water) and trehalose-based (20 % (wt/wt) in saline water) at a ratio of 1:1 were also tested. Results showed no statistically significant loss of either culturability or acidifying activity, regardless the protective conditions (see **ESM Table S4**). The freeze-thaw behaviour of *C. maltaromaticum* seemed no to be influenced by the nature and the concentration of the disaccharides used as cryoprotective agent, within the tested range of conditions.

Cytoplasmic membrane properties

Fatty acid composition of the lipid membrane

The fatty acid compositions of the studied strains are presented in **Table 1**.

C. maltaromaticum CNCM I-3298 lipid membranes are mainly composed of oleic acid (C18:1), accounting for over 80 % of their total fatty acid content. Such a high percentage of C18:1 leads to *C. maltaromaticum* presenting the highest content of long chain fatty acids (87 %) and highest unsaturated to saturate fatty acid ratio (UFA/SFA = 5.60) among the three strains. *L. bulgaricus* ATCC 11842 and *L. bulgaricus* CFL1 lipid membranes are composed of four main types of fatty acids (C14:0, C16:0, C16:1 and C18:1), accounting for over 80 % of their total fatty acid composition. The higher percentage of C18:1 in *L. bulgaricus* ATCC 11842 (26 %) compared to *L. bulgaricus* CFL1 (16 %) also results in a higher UFA/SFA ratio in *L. bulgaricus* ATCC 11842 versus *L. bulgaricus* CFL1 (1.2 *vs* 0.7). *L. bulgaricus* CFL1, the most cryosensitive strain, showed the lowest relative content of UFA among the studied strains.

Membrane fluidity during cooling

The evolution of membrane fluidity for the three bacterial strains in a 25 % sucrose solution as a function of temperature is presented in **Figure 3**. Fluorescence anisotropy is inversely proportional to membrane fluidity: the higher the anisotropy (r) is, the more rigid the membrane is. Regardless of the strain, decreasing temperature from 35 °C to 0 °C resulted in increasing fluorescence anisotropy and thus in membrane rigidification. From 25 °C downwards, *L. bulgaricus* CFL1 cells (CFL1, in green) exhibited higher anisotropy values (lower membrane fluidity) than *L. bulgaricus* ATCC 11842 (ATCC, in red) and *C. maltaromaticum* (CM, in blue) cells, while the latter two exhibited similar anisotropy values at all temperatures above 5 °C. At 0 °C, *C. maltaromaticum* cells presented the lowest anisotropy (and highest membrane fluidity) (0.209), followed by *L. bulgaricus* ATCC 11842 (0.239) and then *L. bulgaricus* CFL1 (0.273).

Membrane lipid phase transition during freezing, assessed by FTIR spectroscopy.

Figure 4 displays the evolution of the $\nu_s CH_2$ peak positions following cooling from 50 °C to -50 °C for all three strains, in a 25 % sucrose solution. Decreasing temperatures resulted in a shift of $\nu_s CH_2$ peak positions to lower wavenumbers. This reflects the lipid membrane's phase transition from a disordered fluid state, referred to as the liquid crystalline phase, to an ordered rigid state, referred to as the gel phase [39]. The first derivative of the $\nu_s CH_2$ curve as a function of temperature was plotted to determine the lipid membrane phase transition temperature during cooling (Ts). The νH_2O peak positions were simultaneously monitored during cooling to determine, for each sample, the temperature of ice nucleation (Tn) as the upshift of the combination water band from approx. 2100 to 2220 cm^{-1} (the data is not shown on Fig. 4, for sake of clarity). The main results derived from these measurements are presented in **Table 2**.

C. maltaromaticum cells exhibited the lowest Ts values (-8.1 °C), followed by *L. bulgaricus* ATCC 11842 (5.6 °C) and then *L. bulgaricus* CFL1 (13.6 °C). At Tn, the ν_sCH_2 frequencies exhibited by *C. maltaromaticum*, *L. bulgaricus* ATCC 11842 and *L. bulgaricus* CFL1 were 2852.8 cm^{-1}, 2850.7 cm^{-1} and 2850.1 cm^{-1}, respectively. This suggests that when ice formation begins, the lipid membrane of *C. maltaromaticum* cells still exhibits a high degree of disorganization and fluidity, whereas the lipid membranes of the other two strains have already transitioned into the gel phase. Regardless of temperature, and especially in the frozen state (temperatures below Tn), *L. bulgaricus* CFL1 cells showed the lowest ν_sCH_2 frequencies (i.e. highest degree of acyl chain organization) among the three strains. The differences in the lipid organization observed among strains at Tn were the same at the frozen state (-48°C)

Intracellular glass transition temperature

Intracellular glass transition temperature measurements of washed cells revealed no significant differences (p <0.05) between the *L. bulgaricus* strains: a median value of -19.3 °C for *L. bulgaricus* ATCC 11842 and of -17.9 °C for *L. bulgaricus* CFL1. The intracellular glass transition temperature of washed *C. maltaromaticum* cells was significantly higher than the other two strains, with a median value of -15.2 °C. However, adding the cryoprotective solution (20 % sucrose in saline water) led to a Tg'i decrease in all three strains, down to not significantly different median values (p < 0.05) for *C. maltaromaticum* (-26.6 °C), *L. bulgaricus* ATCC 11842 (-26.4 °C) and *L. bulgaricus* CFL1 (-27.0 °C).

Differences in biochemical compositions on fresh and freeze-thawed cells, assessed by FTIR micro-spectroscopy

The 3016 – 2800 cm^{-1} spectral region.

PCA was performed on baseline-corrected and normalized water subtracted spectra of fresh cells in the 3016 – 2800 cm^{-1} range. The PC1 versus PC2 score plot, the corresponding PC1 loading plot and the averaged spectra of each strain are reported in **Figures 5a, 5b** and **5c,** respectively.

PCA score plots separated the *C. maltaromaticum* CNCM I-3298 (CM) cluster from the *L. bulgaricus* ATCC 11842 and CFL1 clusters according to PC1 (81% of total variance) and the *L. bulgaricus* ATCC 11842 cluster from the *L. bulgaricus* CFL1 cluster according to PC2 (4 % of total variance). The loading plot of PC1 (**Fig. 5b**) indicates that *C. maltaromaticum* (CM) cells are correlated to CH_2 vibration bands ($\nu_{as}CH_2$ (2935 – 2917cm^{-1}) and ν_sCH_2 (2858 – 2848 cm^{-1})) and C=CH vibration bands (3010 – 2990), while the *L. bulgaricus* cells (ATCC and CFL1) are correlated to CH_3 vibration bands ($\nu_{as}CH_3$ (2972 – 2950cm^{-1}) and ν_sCH_3 (2900 – 2865 cm^{-1})). This can also be seen in the averaged spectra (**Fig. 5c**), where

C. maltaromaticum cells present a higher absorbance in CH_2 vibration bands (2854 cm^{-1}, 2930 cm^{-1}) and lower absorbance in CH_3 vibration bands (2873 cm^{-1}, 2960 cm^{-1}) than the *L. bulgaricus* strains. The averaged spectra, in accordance with the information presented by the loading plot of PC2 (see **ESM Fig. S2**), also show that *L. bulgaricus* ATCC 11842 cells exhibit a higher absorbance in the $\nu_s CH_2$ (2860-2854 cm^{-1}) vibration band than *L. bulgaricus* CFL1 cells.

PCA was also performed by combining the spectra acquired on fresh and thawed samples of the three bacteria (see **ESM Fig. S3a** and **Fig. S3b**). The PC1 versus PC2 and PC1 versus PC3 score plots revealed a separation between the fresh and the thawed samples of *L. bulgaricus* strains, whereas no differentiation was observed for *C. maltaromaticum*. We observed a shift of the *L. bulgaricus* (ATCC and CFL1) thawed samples to positive direction of PC1 and PC2, and an increased dispersion within the bacterial spectra. Freezing and thawing processes would therefore induce a disorganization of the lipid membrane of *L. bulgaricus* strains.

The 1800 – 1370 cm^{-1} region.

PCA was performed on baseline-corrected and normalized water subtracted spectra of fresh cells in the 1800 – 1370 cm^{-1} range. The PC1 versus PC2 score plot and corresponding PC1 and PC2 loading plots are presented in **Figures 6a, 6b** and **6c** respectively.

PCA separated the *C. maltaromaticum* CNCM I-3298 (CM) cluster from the *L. bulgaricus* CFL1 (CFL1) cluster according to PC1 (87 % of total variance) and from the *L. bulgaricus* ATCC 11842 (ATCC) cluster according to PC2 (7 % of total variance). The loading plots of PC1 and PC2 (**Fig. 6b** and **6c**) indicate that cluster discrimination was linked to nucleic acids, Amide I band components and the Amide II band. Furthermore, the fresh samples of *L. bulgaricus* CFL1 exhibited the highest sample's dispersion along PC2 axis.

The potential damaging effect of freezing on protein was investigated by performing PCA using the spectra acquired on fresh and thawed samples of the three bacteria (see **ESM Fig S4**). The thawed samples of *L. bulgaricus* strains were slightly shifted from the fresh samples to negative direction of PC2 (see **ESM Fig S4a**, PC1 versus PC2 score plot). The shift appeared more pronounced for *L. bulgaricus* ATCC 11842 than *L. bulgaricus* CFL1. No separation between the fresh and the frozen samples was observed for *C. maltaromaticum*. The major contribution to spectral variation between fresh and frozen samples of *L. bulgaricus* strains arose from the following bands: 1637 cm^{-1}, corresponding to the β-sheet components of the Amide I bands, and 1753 cm^{-1} (C=O vibrations of esters) (see **ESM Fig. S4c** and **Fig. S4d**).

To further analyze the secondary structure of proteins, the second derivative of the averaged spectra were plotted (**Fig. 6d**) and the ratios of α-helix band intensity at 1654 cm^{-1} over those of β-sheet band

intensity at 1637 cm^{-1} (I_{1654}/I_{1637}) were calculated for fresh and thawed cells of each strain. Results are presented in **Figure 6e**.

When comparing the averaged I_{1654}/I_{1637} ratios measured in fresh cells, *C. maltaromaticum* (CM) cells showed the highest ratio (2.52) among the strains (i.e. the highest content of proteins presenting α-helical structures over β-sheet structures), whereas *L. bulgaricus* ATCC 11842 (ATCC) cells showed the lowest ratio (2.01).

When comparing the average ratios measured between fresh and thawed cells of each strain, *L. bulgaricus* CFL1 cells (the least cryoresistant strain) (CFL1) presented the most significant difference in ratio, followed by *L. bulgaricus* ATCC 11842 cells. *C. maltaromaticum*, the most cryoresistant strain, did not present a significant difference in I_{1654}/I_{1637} ratio between fresh and thawed cells.

The 1370 – 975 cm^{-1} region.

PCA was performed on baseline-corrected and normalized water subtracted spectra of fresh cells in the 1370 – 975 cm^{-1} range. The PC1 versus PC2 score plot and the corresponding loading plots of PC1 and PC2 are reported in **Fig. 7a, 7b** and **7c**, respectively. The averaged spectrum of each strain is plotted in **Fig. 7d**.

The *C. maltaromaticum* CNCM I-3298 (CM) cluster is separated from the *L. bulgaricus* ATCC 11842 (ATCC) cluster along PC1 (87% of variance). The positive peaks in the loading plot of PC1 (**Fig. 7b**) reveal that *L. bulgaricus* ATCC 11842 cells are characterized by spectral features in the 1300 – 1230 cm^{-1} range, encompassing notably the Amide III region of proteins, and the 1112 – 1085 cm^{-1} range, arising from sugar rings, as well as phosphodiester (PO_2^-) functional groups of phospholipids, teichoic acids (charged polymers present in the cell wall of Gram-positive bacteria) or nucleic acid structures [40–42]. The negative peaks in the loading plot of PC1 reveal that *C. maltaromaticum* cells were characterized by spectral features in the 1360 – 1315 and 1185 – 1125 cm^{-1} ranges, as well as a higher contribution of complex sugar ring modes in the 1060 – 1044 cm^{-1} range, arising from the peptidoglycan of the cell wall [42,43].

The most cryosensitive strain, *L. bulgaricus* CFL1, is separated from the other two strains along PC2 (10 % of total variance). The negative peaks in the loading plot of PC2 (**Fig. 7c**) reveal that *L. bulgaricus* CFL1 cells were characterized by a higher contribution of PO_2^- groups (1235 – 1205 cm^{-1}; 1090 – 1075 cm^{-1}).

The 1200 – 975 cm^{-1} region.

PCA was performed in the 1200 – 975 cm^{-1} region mainly containing information on cell wall components (PO_2^- groups and sugar rings) and nucleic acid (PO_2^- groups) using spectra of fresh and

thawed samples (**Fig. 8**). The contribution from membrane phospholipids to the PO_2^- groups' vibration band is expected to be small, given the Gram-positive bacteria membrane is composed of a single lipid bilayer with associated proteins [42]. The PC1 versus PC3 score plot revealed no cluster for *C. maltaromaticum* (CM) between fresh and thawed samples, whereas a separation was observed for *L. bulgaricus* strains (**Fig. 8a**). The separation between fresh and thawed samples appeared more pronounced for the *L. bulgaricus* CFL1 cells than for the *L. bulgaricus* ATCC 11842 cells, with a shift of thawed samples to the negative direction of PC3. The loading plot of PC3 (**Fig. 8b**) indicated that thawed samples of *L. bulgaricus* were characterized by a higher spectral contribution of some bands associated with sugar rings vibrations (1064 – 1052 cm^{-1} and 1037 cm^{-1}). **Figure 8c** displayed the averaged second derivative of fresh and thawed samples for the three strains and enables better identification of the spectral changes induced by the freeze-thaw process. Freezing resulted in several modifications in this spectral region: i) a decrease in the peak height of the vibration bands at 1120 cm^{-1} (sugars) and 1085 cm^{-1} (phosphodiester (PO_2^-) groups); ii) a slight increase of the peak height at 1058 cm^{-1} (sugars); and iii) for the vibration band at 1037 cm^{-1}, an increase of the peak height for *L. bulgaricus* ATCC 11842, but a shift to lower wavenumber for *L. bulgaricus* CFL1.

Discussion

The interest for lactic acid bacteria (LAB) has been continuously growing, particularly because of their probiotic properties. However, some promising bacteria remain under-exploited due to their inability to overcome the environmental stresses induced by stabilization processes. Even if freezing is widely used for preserving LAB, some irreversible losses of functionality and viability are still observed. By comparing the properties of three LAB exhibiting various levels of freeze-sensitivity – *C. maltaromaticum* CNCM I-3298 (displaying the highest cryoresistance), *L. bulgaricus* ATCC 11842 (displaying intermediate cryoresistance) and *L. bulgaricus* CFL1 (displaying the lowest cryoresistant)) – our objective is to better understand the cellular damage induced by freezing as well as to identify markers of cryoresistance that could be used for screening LAB strains.

The major physical events that take place during the slow freezing of LAB have been well described by Fonseca et al. [1] and Meneghel et al. [2], according to four main physical properties: i) membrane lipid phase transition temperature following cooling (Ts); ii) ice nucleation temperature (Tn); iii) intracellular glass transition temperature (Tg'i); and iv) extracellular glass transition temperature (Tg'e). To discuss the relevance of these properties to explain the freeze-resistance, a dynamic representation of the behavior of the three bacterial cells following freezing from the growth temperature to -80°C is shown in **Fig. 9**. Schematic drawings of the physical state of the cells are also included. After growth, LAB membranes are in a fluid crystalline phase and following cooling, they change to a gel state (at Ts). At approximately −10 °C (Tn), ice nucleation occurs and the formation of ice crystals in the extracellular medium begins. The cryoconcentration of the extracellular matrix results in water efflux from the cell and in cell volume reduction (cell dehydration). Cell dehydration ceases at Tg'i with the vitrification of the intracellular matrix. Cells thus become osmotically irresponsive to the extracellular medium [1]. At Tg'e, the vitrification of the extracellular medium occurs and the bacteria are immobilized in a high viscous matrix (glassy state) where diffusive damaging reactions are prevented, due to the low molecular mobility characterizing this state. When comparing the three LAB of this study, the main difference is the value of their membrane lipid phase transition temperature (Ts). The membrane of *L. bulgaricus* CFL1 and ATCC 11842 is in the gel phase during the event of cell dehydration induced by the cryoconcentration of the extracellular medium (osmotic stress), whereas the membrane of *C. maltaromaticum* remains more fluid in the liquid crystalline state. The higher membrane fluidity of *C. maltaromaticum* at subzero temperature is also confirmed by the highest wavenumber of $\nu_s CH_2$ at ice nucleation temperature and at -48 °C (**Table 2**), as well as by the lowest value of fluorescence anisotropy (r) at 0 °C (highest membrane fluidity, **Fig. 3**).

Freezing can be considered as a combination of different stresses applied to bacterial cells: exposure to cold temperatures, ice formation, and high solutes concentration. Osmotic stress has been reported as the main source of cellular damage for the most freeze-sensitive bacteria, *L. bulgaricus* CFL1 [2]. The

maintenance of a more fluid and flexible membrane around water nucleation temperature facilitates water efflux from the intracellular medium and cell volume reduction, thus limiting mechanical constraints on the cell membrane during freezing.

Several authors used the UFA/SFA ratio for assessing membrane fluidity and correlated the improvement of LAB freeze-resistance with change in membrane composition, in particular with higher UFA/SFA ratio and/or higher content of CFA (**Table S1**) [12]. The data from the studies reported in **Table S1** have been used to calculate the UFA/SFA ratio (excluding CFA) and to plot the survival rate obtained after freezing as a function of the UFA/SFA ratio (**Fig. 10a**). For CFA contents lower than 10%, the survival rate appears to be positively correlated with the UFA/SFA ratio, which is not the case when CFA contents are higher than 10 % of the FA composition. However, the increase of CFA content in membrane fatty acid composition seems to result in increasing the survival rate after freezing (**Fig. 10b**). The contribution of CFA to LAB cryoresistance might thus be linked to the presence of other lipid types in the cell membrane. One study reported increased cryoresistance with increased CFA contents in strains natively low in UFA; and conversely, decreased cryoresistance with increased CFA contents in strains natively high in UFA [13]. The effect of CFA, as well as the UFA/SFA ratio on both LAB cryoresistance and membrane properties, remains unclear and requires additional studies.

Lactococcus lactis subsp. *lactis* TOMSC161 has been reported as freeze-resistant while exhibiting a UFA/SFA ratio of 0.1, a CFA content of 35 % and a Ts value of 13 °C [44]. Bacterial resistance to osmotic stress occurring during freezing is influenced not only by membrane properties and membrane fluidity but also by cell morphology (size and shape). Some studies have related bacterial freeze-sensitivity to the surface area-to-volume ratio of cells [45,46]. For instance, the freeze-sensitive lactobacilli strain *L. bulgaricus* CFL1, exhibited a surface area-to-volume ratio three to four times lower than strains of *Streptococcus thermophilus*, a freeze-resistant species of LAB [45].

Cryoconcentration of the extracellular medium (osmotic stress) being the most damaging stress for LAB during freezing [2], the bacterial membrane appears as the first target of injury due to its proximity to the extracellular medium. Most studies investigating the cryoinjury of bacterial cells reported a loss of membrane integrity, membrane permeabilization, and leakage of intracellular contents when slow cooling rates were applied [3–5,47,48].

An alteration of cell wall components was also evidenced after exposure to osmotic stress [49]. Growth of *Lactobacillus casei* in high salt conditions (1 M NaCl) modified the structural properties of its peptidoglycan layer (decrease in the cross-linking degree) [49]. In this work, we have evidenced by probing bacterial populations with FTIR micro-spectroscopy, that the freeze-thaw process induced not only changes in membrane lipid components (spectral region 3016-2800 cm^{-1}), but also in proteins (1700 – 1600 cm^{-1}) and the peptidoglycan cell wall (1200 – 1000 cm^{-1}). Furthermore, the cellular damage

induced by freezing seemed to increase heterogeneity within the freeze-thawed bacterial populations (**Fig. S3a, S4a, 8a**).

FTIR spectroscopy techniques have already been used to investigate biochemical changes induced by freezing of LAB (analysis of LAB cells in the dried state) [6], or by exposure to environmental modifications of LAB (drying processes [50]; zinc exposure [51]) or other microorganisms (thermal stress [28]; cold stress [30], silver ions stress [31]; air-drying of yeast [32]). A loss of α-helical proteins structures and/or an increase in β-sheet (or β-turns) structures were noticed in most studies, suggesting protein denaturation after applying the stressful treatment to the microbial population. A recent phenotypic and genotypic study of *L. crispatus* and *L. gasseri* strains revealed a possible implication of membrane protein transport systems in resistance of osmotic and ionic stresses, as well as of exposure to antibiotics and metals [52]. The potential link between the denaturation of these protein systems and the loss of bacterial resistance deserved further investigation. Alteration of cell wall polysaccharides and nucleic acids were also observed [28,30,32,50,51]. Damage of nucleic acids was assessed by investigating the spectral region associated with the asymmetric and symmetric PO_2^- stretching vibration at approximately 1220 cm^{-1} and 1080 cm^{-1}, respectively. Even if the PO_2^- groups are present in the phosphodiester functional groups of DNA/RNA polysaccharide backbones, they are also involved in the polar head groups of phospholipids and phosphorus-containing carbohydrates such as teichoic acids and lipoteichoic acids (charged polymers present in the cell wall of Gram-positive bacteria). Kochan et al. [42] investigated by atomic force microscopy-infrared (AFM-IR) spectroscopy the cell-wall signature of Gram-positive and Gram-negative bacteria, as well as the dynamical changes occurring in the cell wall during cell division of *Staphylococcus aureus* (Gram-positive bacteria). Their results indicated that when considering Gram-positive bacteria, the changes observed in the spectral range of PO_2^- group vibrations are mostly ascribed to cell wall components. Further studies are thus required to evidence potential damage of nucleic acids following freeze-thawing of LAB. The cell wall seemed also to be involved in *Lactobacillus* resistance to exposure to Zn^{2+} [51] and heavy metals [53,54]. Modification of *L. plantarum* cell surface components were detected in the presence of Zn2+ by applying FTIR spectroscopy and electronic microscopy [51]. However, no change of membrane surface properties was detected on several strains of *Lactobacillus* after exposure to lead and cadmium [55].

The FTIR microscopic approach developed by Meneghel et al. [33] for analysing samples in an aqueous environment not only enables the identification of cellular damage induced by freezing but also the discrimination of bacterial populations before freezing. The three investigated LAB exhibited different biochemical compositions regardless of the spectral regions considered, and thus the cellular components (lipid membrane, protein, cell wall, **Fig. 5, 6** and **7**). The largest spectral differences among the strains were measured in the 1370 – 975 cm^{-1} region (**Fig. 7**). This region harbors information arising from the Amide III band as well as cell wall components, such as phosphate-containing cellular compounds (i.e. teichoic acids) and complex sugar rings of the peptidoglycan [40–42]. The more

cryoresistant strains (*C. maltaromaticum* and *L. bulgaricus* ATCC 11842) were characterized by higher absorbance bands arising from complex sugar ring modes of the peptidoglycan compared to the cryosensitive strain, suggesting that the peptidoglycan is likely involved in cryoresistance mechanisms. By acquiring infrared spectra and cryoresistance data on new LAB (or in LAB grown and or protected in different conditions), it could be possible to apply statistical approaches developed for identifying bacteria species based on infrared spectra [56–59] and thus to classify the bacteria according to their degree of freeze-tolerance by considering their proximity to the cryoresistant LAB *C. maltaromaticum*, or the cryosensitive LAB, *L. bulgaricus* CFL1. The information directly gathered from the FTIR micro-spectroscopy spectra (i.e. protein conformation, cell wall composition) and through multivariate analysis could be used as a fast screening method for selecting adequate culture conditions, composition of protective solution, or freezing conditions that improve the freezing resistance of a given bacteria, before confirming with freeze-thaw biological activity measurements. This approach could be easily enlarged to the investigation and understanding of micro-organisms resistance to various stressors.

Conclusions

Our work focused on the in-depth characterization of three lactic acid bacteria exhibiting different levels of sensitivity to the freezing process using multiple analytical methods. Classical methods used for determining fatty acid composition or membrane fluidity, as well as a recently developed FTIR micro-spectroscopy approach allowing the study of the whole mid-infrared region of live bacteria, in their aqueous environment, were applied to understand the cellular damage induced by freezing and identify markers of cryoresistance. We proposed in **Table 3**, a list of markers. Some were already reported in the literature such as the UFA/SFA ratio, the lipid membrane phase transition temperature (Ts), while others are new, and coming from the multivariate analysis of infrared spectra performed in this work. For LAB exhibiting low membrane content of CFA (lower than 10 %), cryoresistant cells can be mainly characterized by a UFA/SFA ratio higher than 1.5, a Ts value lower than 0 °C, and an anisotropy ratio between 0 °C and 35 °C lower than 1.5. These properties favor the maintenance of a high degree of membrane fluidity at low temperatures when ice nucleation occurs. The FTIR-microspectroscopy results evidenced the cellular damage induced by freeze-thawing, especially an alteration of protein conformation and the peptidoglycan cell wall. A reduction in the α-helical over β-sheet band intensities (I_{1654}/I_{1637} ratio), as well as intensity reductions in bands corresponding to cell wall components (1120 cm^{-1} and 1085 cm^{-1}) were observed after freeze-thawing in the freeze-sensitive *L. bulgaricus* ATCC 11842 and CFL1 populations. The absorbance intensity changes of these specific spectral bands following freezing were proposed as new markers of cryoresistance. Although the membrane fatty acid composition is the most documented property in literature, systematic studies relating LAB cryoresistance to their membrane physical properties and FTIR spectra before and after freeze-thawing become essential for confirming and enriching the proposed cellular markers of cryoresistance.

Declarations

Acknowledgments and Funding Information

This work has received funding from the European Union's Horizon 2020 research and innovation program under grant agreement N° 777657.

Compliance with ethical standards: This article does not contain any studies with human participants or animals performed by any of the authors.

Conflict of interest: There are no conflict of interest to declare

Data availability: The datasets generated and/or analysed during the current study are available in the Data INRAE repository at https://doi.org/10.15454/ILMSYG.

Authors' contributions

Conceptualization, AG, SP and FF; methodology, JM, AG, SP and FF; investigation and validation AG, JM, SC, PL and FF; data curation, AG, SC, SP and FF; formal analysis, AG, SC, PL and FF; writing original draft of the paper, AG, FF, SP; writing-review, SP, FF; final review and editing, AG, JM, ICT, SP, FF; supervision and project administration, SP, FF; resources and funding acquisition, SP, I-CT, FF.

Consent for publication

All authors had full access to the data and have read and approved the manuscript before submission

Table 1 Membrane fatty acid composition (relative percentages) of *C. maltaromaticum* CNCM I-3298, *L. bulgaricus* ATCC 11842 and *L. bulgaricus* CFL1 and cells. Values for *L. bulgaricus* ATCC 11842 and *L. bulgaricus* CFL1 were recalculated from raw data available from Meneghel et al. [2]

Fatty acids (%)	*C. maltaromaticum* CNCM I-3298	*L. bulgaricus* ATCC 11842	*L. bulgaricus* CFL1
C12:0	0.3 ^{c}	3.3 ^{a}	1.9 ^{b}
C14:0	1.9 ^{c}	6.9 ^{b}	10.3 ^{a}
C15:0	0.2 ^{b}	0.8 ^{a}	0.7 ^{a}
C16:0	10.7 ^{c}	25.4 ^{b}	36.7 ^{a}
C16:1	0.2 ^{b}	23.8 ^{a}	22.2 ^{a}
C17:0	0.15 ^{b}	0.3 ^{a}	0.1 ^{b}
C18:0	1.6 ^{b}	6.2 ^{a}	7.0 ^{a}
C18:1	82.8 ^{a}	26.2 ^{b}	15.9 ^{c}
C18:2	0.0 ^{c}	2.0 ^{a}	1.5 ^{b}
C19cyc	0.0 ^{c}	4.6 ^{a}	3.1 ^{b}
C20:0	0.0 ^{b}	0.2 ^{a}	0.1 ^{a}
C18:2 conj	1.8 ^{a}	0.1 ^{b}	0 ^{c}
C22:0	0.3 ^{b}	0.3 ^{b}	0.5 ^{a}
Total SFA*	15.2 ^{c}	43.4 ^{b}	57.2 ^{a}
Total UFA**	84.9 ^{a}	50.2 ^{b}	38 ^{c}
UFA/SFA	5.6 ^{a}	1.2 ^{b}	0.7 ^{c}
Total long chain FA***	86.7 ^{a}	39.8 ^{b}	28.3 ^{c}

Data presented are means of at least three independent replicates
Superscript letters (a, b, c) represent statistical differences for each fatty acid between strains at the 95 % confidence level.
SFA: Saturated Fatty Acids; UFA: Unsaturated Fatty Acids
* Totals include fatty acids not shown in the table, representing less than 1 % of total FA
** Total UFA does not comprise C19:0cyc
*** Long chain FA comprise fatty acids made up of 18 carbon atoms or more

Table 2 Main parameters characterizing membrane lipid phase transition of *C. maltaromaticum* CNCM I-3298, *L. bulgaricus* ATCC 11842 and *L. bulgaricus* CFL1 cells obtained by monitoring the peak position of $\nu_s CH_2$ around 2850 cm^{-1} (Ts and $\nu_s CH_2$) and the upshift of the vibration water band from approx. 2100 to 2220 cm^{-1} during cooling (Tn) (**Fig.5**)

	C. maltaromaticum CNCM I-3298	*L. bulgaricus* ATCC 11842	*L. bulgaricus* CFL1
Ts (°C)	-8.1 [a]	5.6 [b]	13.6 [c]
Tn (°C)	-9.6 [a]	-13.6 [a]	-10.2 [a]
$\nu_s CH_2$ at Tn (cm^{-1})	2852.8 [a]	2850.7 [b]	2850.1 [c]
$\nu_s CH_2$ at -48°C (cm^{-1})	2851.5 [a]	2850.1 [b]	2849.4 [c]

Data presented are medians of three independent replicates for each strain
Superscript letters (a, b, c) represent statistical differences, for each parameter, between strains at the 95 % confidence level
Ts: lipid membrane phase transition temperature during cooling
Tn: water nucleation temperature

Table 3 Summary of the markers of LAB cryoresistance put forward in this study, according to the analytical method employed

Methods	**Markers of cryoresistance**
Membrane fatty acid composition	UFA/SFA > 1.5 for CFA < 10 %* Or CFA > 20 % *
Lipid membrane phase transition Symmetric CH_2 stretching vibration band (νsCH_2)	Ts < 0 °C (CFA < 10 %) νsCH_2 frequency at -48 °C > 2850 cm^{-1}
Fluorescence anisotropy (r)	Ratio between the anisotropy values at 0°C and 35 °C (r_0/r_{35}) < 1.5
FTIR microscopy in aqueous conditions (before and after freeze-thawing process)	No reduction of the ratio I_{1654}/I_{1637} after freeze-thawing (or difference lower than 0.1 compared to the fresh cells) No reduction of the absorbance of the spectral bands at 1120 cm^{-1} and 1085 cm^{-1} after freeze-thawing

* survival rate higher than 50 % (Fig. 11)

UFA: unsaturated fatty acids; SFA: saturated fatty acids; CFA: cyclic fatty acids; UFA/SFA does not include CFA; Ts: lipid membrane phase transition temperature following freezing

References

1. Fonseca F, Meneghel J, Cenard S, Passot S, Morris GJ. Determination of intracellular vitrification temperatures for unicellular micro-organisms under conditions relevant for cryopreservation. Rubinsky B, editor. PLOS ONE [Internet]. 2016 [cited 2018 Nov 2];11:e0152939. Available from: https://dx.plos.org/10.1371/journal.pone.0152939

2. Meneghel J, Passot S, Dupont S, Fonseca F. Biophysical characterization of the *Lactobacillus delbrueckii* subsp. *bulgaricus* membrane during cold and osmotic stress and its relevance for cryopreservation. Appl Microbiol Biotechnol [Internet]. 2017 [cited 2020 Mar 16];101:1427–41. Available from: http://link.springer.com/10.1007/s00253-016-7935-4

3. Fernandez ML, Cabrera GM, de Valdez GF, Disalvo A, Seldes AM. Influence of growth temperature on cryotolerance and lipid composition of *Lactobacillus acidophilus*. J Appl Microbiol [Internet]. 2000 [cited 2018 Nov 1];88:342–8. Available from: http://doi.wiley.com/10.1046/j.1365-2672.2000.00967.x

4. Rault A, Béal C, Ghorbal S, Ogier J-C, Bouix M. Multiparametric flow cytometry allows rapid assessment and comparison of lactic acid bacteria viability after freezing and during frozen storage. Cryobiology [Internet]. 2007 [cited 2015 Feb 4];55:35–43. Available from: http://linkinghub.elsevier.com/retrieve/pii/S0011224007000612

5. Gautier J, Passot S, Pénicaud C, Guillemin H, Cenard S, Lieben P, et al. A low membrane lipid phase transition temperature is associated with a high cryotolerance of *Lactobacillus delbrueckii* subsp. *bulgaricus* CFL1. J Dairy Sci [Internet]. 2013 [cited 2018 Nov 2];96:5591–602. Available from: http://linkinghub.elsevier.com/retrieve/pii/S0022030213004682

6. Passot S, Gautier J, Jamme F, Cenard S, Dumas P, Fonseca F. Understanding the cryotolerance of lactic acid bacteria using combined synchrotron infrared and fluorescence microscopies. The Analyst [Internet]. 2015 [cited 2018 Nov 2];140:5920–8. Available from: http://xlink.rsc.org/?DOI=C5AN00654F

7. Cárcoba R, Rodriguez A. Influence of cryoprotectants on the viability and acidifying activity of frozen and freeze-dried cells of the novel starter strain *Lactococcus lactis* ssp. *lactis* CECT 5180. Eur Food Res Technol [Internet]. 2000 [cited 2015 Feb 4];211:433–7. Available from: http://link.springer.com/article/10.1007/s002170000194

8. Fonseca F, Béal C, Mihoub F, Marin M, Corrieu G. Improvement of cryopreservation of *Lactobacillus delbrueckii* subsp. *bulgaricus* CFL1 with additives displaying different protective effects. Int Dairy J [Internet]. 2003;67:83–90. Available from: https://doi.org/10.1016/S0958-6946(03)00119-5

9. Wang G, Yu X, Lu Z, Yang Y, Xia Y, Lai PF-H, et al. Optimal combination of multiple cryoprotectants and freezing-thawing conditions for high lactobacilli survival rate during freezing and frozen storage. LWT [Internet]. 2019 [cited 2021 Aug 10];99:217–23. Available from: https://linkinghub.elsevier.com/retrieve/pii/S0023643818307977

10. Fonseca F, Béal C, Corrieu G. Operating conditions that affect the resistance of lactic acid bacteria to freezing and frozen storage. Cryobiology [Internet]. 2001;43:189–98. Available from: https://doi.org/10.1006/cryo.2001.2343

11. Fonseca F, Marin M, Morris GJ. Stabilization of frozen *Lactobacillus delbrueckii* subsp. *bulgaricus* in glycerol suspensions: freezing ksinetics and storage temperature effects. Appl Environ Microbiol [Internet]. 2006;72:6474–82. Available from: https://journals.asm.org/doi/10.1128/AEM.00998-06

12. Fonseca F, Pénicaud C, Tymczyszyn EE, Gómez-Zavaglia A, Passot S. Factors influencing the membrane fluidity and the impact on production of lactic acid bacteria starters. Appl Microbiol

Biotechnol [Internet]. 2019 [cited 2021 Aug 10];103:6867–83. Available from: http://link.springer.com/10.1007/s00253-019-10002-1

13. Gómez-Zavaglia A, Disalvo EA, De Antoni GL. Fatty acid composition and freeze-thaw resistance in lactobacilli. J Dairy Res [Internet]. 2000;67:241–7. Available from: https://doi.org/10.1017/S0022029900004179

14. Gilliland SE, Speck ML. Relationship of cellular components to the stability of concentrated lactic *Streptococcus* cultures at -17 C. Appl Microbiol. 1974;4.

15. Smittle RB, Gilliland SE, Speck ML, Walter WMJ. Relationship of cellular fatty acid composition to survival of *Lactobacillus bulgaricus* in liquid nitrogen. Appl Microbiol [Internet]. 1974;27:738–43. Available from: https://doi.org/10.1128/am.27.4.738-743.1974

16. Goldberg I, Eschar L. Stability of lactic acid bacteria to freezing as related to their fatty acid composition. Appl Environnmental Microbiol [Internet]. 1977;33:489--496. Available from: https://doi.org/10.1128/aem.33.3.489-496.1977

17. Broadbent JR, Lin C. Effect of heat shock or cold shock treatment on the resistance of *Lactococcus lactis* to freezing and lyophilization. Cryobiology [Internet]. 1999 [cited 2018 Nov 1];39:88–102. Available from: http://linkinghub.elsevier.com/retrieve/pii/S0011224099921909

18. Wang Y, Corrieu G, Béal C. Fermentation pH and temperature influence the cryotolerance of *Lactobacillus acidophilus* RD758. J Dairy Sci [Internet]. 2005 [cited 2021 Aug 10];88:21–9. Available from: https://linkinghub.elsevier.com/retrieve/pii/S0022030205726588

19. Passot S, Jamme F, Refregiers M, Gautier J, Cenard S, Fonseca F. Synchrotron UV fluorescence microscopy for determining membrane fluidity modification of single bacteria with temperature. Biomed Spectrosc Imaging [Internet]. 2014 [cited 2018 Nov 2];203–10. Available from: http://www.medra.org/servlet/aliasResolver?alias=iospress&genre=article&issn=2212-8794&volume=3&issue=3&spage=203&doi=10.3233/BSI-140062

20. Béal C, Fonseca F, Corrieu G. Resistance to freezing and frozen storage of *Streptococcus thermophilus* is related to membrane fatty acid composition. J Dairy Sci [Internet]. 2001 [cited 2018 Nov 2];84:2347–56. Available from: http://linkinghub.elsevier.com/retrieve/pii/S0022030201746838

21. Wang Y, Delettre J, Guillot A, Corrieu G, Béal C. Influence of cooling temperature and duration on cold adaptation of *Lactobacillus acidophilus* RD758. Cryobiology [Internet]. 2005 [cited 2015 Feb 4];50:294–307. Available from: http://linkinghub.elsevier.com/retrieve/pii/S0011224005000362

22. Wang Y, Delettre J, Corrieu G, Béal C. Starvation induces physiological changes that act on the cryotolerance of *Lactobacillus acidophilus* RD758. Biotechnol Prog [Internet]. 2011 [cited 2018 Nov 1];27:342–50. Available from: http://doi.wiley.com/10.1002/btpr.566

23. Kim WS, Dunn NW. Identification of a cold shock gene in lactic acid bacteria and the effect of cold shock on cryotolerance. Curr Microbiol [Internet]. 1997;35:59–63. Available from: https://doi.org/10.1007/s002849900212

24. Derzelle S, Hallet B, Ferain T, Delcour J, Hols P. Improved adaptation to cold-shock, stationary-phase, and freezingstresses in *Lactobacillus plantarum* overproducing cold-shock proteins. Appl Environ Microbiol [Internet]. 2003 [cited 2015 Feb 4];69:4285–90. Available from: http://aem.asm.org/cgi/doi/10.1128/AEM.69.7.4285-4290.2003

25. Streit F, Delettre J, Corrieu G, Béal C. Acid adaptation of *Lactobacillus delbrueckii* subsp. *bulgaricus* induces physiological responses at membrane and cytosolic levels that improves

cryotolerance. J Appl Microbiol [Internet]. 2008 [cited 2015 Feb 4];105:1071–80. Available from: http://doi.wiley.com/10.1111/j.1365-2672.2008.03848.x

26. Wouters JA, Jeynov B, Rombouts FM, de Vos WM, Kuipers OP, Abee T. Analysis of the role of 7 kDa cold-shock proteins of *Lactococcus lactis* MG1363 in cryoprotection. Microbiology [Internet]. 1999 [cited 2021 Aug 10];145:3185–94. Available from: https://www.microbiologyresearch.org/content/journal/micro/10.1099/00221287-145-11-3185

27. Keto-Timonen R, Hietala N, Palonen E, Hakakorpi A, Lindström M, Korkeala H. Cold Shock Proteins: A Minireview with Special Emphasis on Csp-family of *Enteropathogenic Yersinia* . Front Microbiol [Internet]. 2016 [cited 2021 Aug 10];7. Available from: http://journal.frontiersin.org/Article/10.3389/fmicb.2016.01151/abstract

28. Al-Qadiri HM, Lin M, Al-Holy MA, Cavinato AG, Rasco BA. Detection of sublethal thermal injury in *Salmonella enterica*serotype typhimurium and *Listeria monocytogenes* using Fourier transform infrared (FT-IR) spectroscopy (4000 to 600 cm^{-1}). J Food Sci [Internet]. 2008 [cited 2021 Aug 10];73:M54–61. Available from: https://onlinelibrary.wiley.com/doi/10.1111/j.1750-3841.2007.00640.x

29. Al-Qadiri HM, Al-Alami NI, Al-Holy MA, Rasco BA. Using Fourier transform infrared (FT-IR) absorbance spectroscopy and multivariate analysis to study the effect of chlorine-induced bacterial injury in water. J Agric Food Chem [Internet]. 2008 [cited 2015 Feb 4];56:8992–7. Available from: http://pubs.acs.org/doi/abs/10.1021/jf801604p

30. Lu X, Liu Q, Wu D, Al-Qadiri HM, Al-Alami NI, Kang D-H, et al. Using of infrared spectroscopy to study the survival and injury of *Escherichia coli* O157:H7, *Campylobacter jejuni* and *Pseudomonas aeruginosa* under cold stress in low nutrient media. Food Microbiol [Internet]. 2011 [cited 2015 Feb 4];28:537–46. Available from: http://linkinghub.elsevier.com/retrieve/pii/S0740002010002844

31. Saulou C, Jamme F, Girbal L, Maranges C, Fourquaux I, Cocaign-Bousquet M, et al. Synchrotron FTIR microspectroscopy of *Escherichia coli* at single-cell scale under silver-induced stress conditions. Anal Bioanal Chem [Internet]. 2013 [cited 2015 Feb 4];405:2685–97. Available from: http://link.springer.com/10.1007/s00216-013-6725-4

32. Pénicaud C, Landaud S, Jamme F, Talbot P, Bouix M, Ghorbal S, et al. Physiological and biochemical responses of *Yarrowia lipolytica* to dehydration induced by air-drying and freezing. McNeil P, editor. PLoS ONE [Internet]. 2014 [cited 2018 Nov 2];9:e111138. Available from: https://dx.plos.org/10.1371/journal.pone.0111138

33. Meneghel J, Passot S, Jamme F, Lefrançois S, Lieben P, Dumas P, et al. FTIR micro-spectroscopy using synchrotron-based and thermal source-based radiation for probing live bacteria. Anal Bioanal Chem [Internet]. 2020 [cited 2020 Nov 19];412:7049–61. Available from: http://link.springer.com/10.1007/s00216-020-02835-x

34. Walker VK, Palmer GR, Voordouw G. Freeze-thaw tolerance and clues to the winter survival of a soil community. Appl Environ Microbiol [Internet]. 2006 [cited 2021 Aug 10];72:1784–92. Available from: https://journals.asm.org/doi/10.1128/AEM.72.3.1784-1792.2006

35. Girardeau A, Puentes C, Keravec S, Peteuil P, Trelea IC, Fonseca F. Influence of culture conditions on the technological properties of *Carnobacterium maltaromaticum* CNCM I-3298 starters. J Appl Microbiol [Internet]. 2019 [cited 2021 Aug 10];126:1468–79. Available from: https://onlinelibrary.wiley.com/doi/10.1111/jam.14223

36. Clarke A, Morris GJ, Fonseca F, Murray BJ, Acton E, Price HC. A low temperature limit for life on earth. Neufeld J, editor. PLoS ONE [Internet]. 2013 [cited 2018 Nov 2];8:e66207. Available from: https://dx.plos.org/10.1371/journal.pone.0066207

37. Vaccari L, Birada G, Grenci G, Pacor S, Businaro L. Synchrotron radiation infrared microspectroscopy of single living cells in microfluidic devices: advantages, disadvantages and future perspectives. J Phys Conf Ser [Internet]. 2012 [cited 2020 Mar 16];359:012007. Available from: http://stacks.iop.org/1742-6596/359/i=1/a=012007?key=crossref.39973d303808f08f77a36f800ba33ed4

38. Afseth NK, Kohler A. Extended multiplicative signal correction in vibrational spectroscopy, a tutorial. Chemom Intell Lab Syst [Internet]. 2012 [cited 2015 Feb 4];117:92–9. Available from: http://linkinghub.elsevier.com/retrieve/pii/S0169743912000494

39. Wolkers WF, Oldenhof H. Use of *in situ* Fourier transform infrared spectroscopy to study freezing and drying of cells. In: Wolkers WF, Oldenhof H, editors. Cryopreserv Free-Dry Protoc [Internet]. New York, NY: Springer New York; 2015 [cited 2015 Feb 4]. p. 147–61. Available from: http://link.springer.com/10.1007/978-1-4939-2193-5_5

40. Quilès F, Humbert F, Delille A. Analysis of changes in attenuated total reflection FTIR fingerprints of *Pseudomonas fluorescens* from planktonic state to nascent biofilm state. Spectrochim Acta A Mol Biomol Spectrosc [Internet]. 2010 [cited 2020 Mar 16];75:610–6. Available from: https://linkinghub.elsevier.com/retrieve/pii/S1386142509006027

41. Lasch P, Naumann D. Infrared Spectroscopy in Microbiology. In: Meyers RA, editor. Encycl Anal Chem [Internet]. Chichester, UK: John Wiley & Sons, Ltd; 2015 [cited 2020 Mar 29]. p. 1–32. Available from: http://doi.wiley.com/10.1002/9780470027318.a0117.pub2

42. Kochan K, Perez-Guaita D, Pissang J, Jiang J-H, Peleg AY, McNaughton D, et al. *In vivo* atomic force microscopy–infrared spectroscopy of bacteria. J R Soc Interface [Internet]. 2018 [cited 2021 Aug 10];15:20180115. Available from: https://royalsocietypublishing.org/doi/10.1098/rsif.2018.0115

43. Naumann D, Barnickel G, Bradaczek H, Labischinski H, Giesbrecht P. Infrared spectroscopy, a tool for probing bacterial peptidoglycan: Potentialities of infrared spectroscopy for cell wall analytical studies and rejection of models based on crystalline chitin. Eur J Biochem [Internet]. 1982 [cited 2020 Mar 16];125:505–15. Available from: http://doi.wiley.com/10.1111/j.1432-1033.1982.tb06711.x

44. Velly H, Bouix M, Passot S, Penicaud C, Beinsteiner H, Ghorbal S, et al. Cyclopropanation of unsaturated fatty acids and membrane rigidification improve the freeze-drying resistance of *Lactococcus lactis* subsp. *lactis* TOMSC161. Appl Microbiol Biotechnol [Internet]. 2015 [cited 2018 Nov 2];99:907–18. Available from: http://link.springer.com/10.1007/s00253-014-6152-2

45. Fonseca F, Béal C, Corrieu G. Method of quantifying the loss of acidification activity of lactic acid starters during freezing and frozen storage. J Dairy Res [Internet]. 2000;67:83–90. Available from: https://doi.org/10.1017/S002202999900401X

46. Dumont F, Marechal P-A, Gervais P. Cell size and water permeability as determining factors for cell viability after freezing at different cooling rates. Appl Environ Microbiol [Internet]. 2004 [cited 2015 Feb 4];70:268–72. Available from: http://aem.asm.org/cgi/doi/10.1128/AEM.70.1.268-272.2004

47. Moussa M, Dumont F, Perrier-Cornet J-M, Gervais P. Cell inactivation and membrane damage after long-term treatments at sub-zero temperature in the supercooled and frozen states. Biotechnol Bioeng [Internet]. 2008 [cited 2021 Aug 10];101:1245–55. Available from: https://onlinelibrary.wiley.com/doi/10.1002/bit.21981

48. Simonin H, Bergaoui IM, Perrier-Cornet JM, Gervais P. Cryopreservation of *Escherichia coli* K12TG1: Protection from the damaging effects of supercooling by freezing. Cryobiology [Internet]. 2015 [cited 2021 Aug 10];70:115–21. Available from: https://linkinghub.elsevier.com/retrieve/pii/S0011224014007123

49. Piuri M, Sanchez-Rivas C, Ruzal SM. Cell wall modifications during osmotic stress in *Lactobacillus casei*. J Appl Microbiol [Internet]. 2005 [cited 2021 Aug 10];98:84–95. Available from: https://onlinelibrary.wiley.com/doi/10.1111/j.1365-2672.2004.02428.x

50. Hlaing MM, Wood BR, McNaughton D, Ying D, Dumsday G, Augustin MA. Effect of drying methods on protein and DNA conformation changes in *Lactobacillus rhamnosus* GG cells by Fourier transform infrared spectroscopy. J Agric Food Chem [Internet]. 2017 [cited 2021 Aug 10];65:1724–31. Available from: https://pubs.acs.org/doi/10.1021/acs.jafc.6b05508

51. Mohd Yusof H, Mohamad R, Zaidan UH, Rahman NA. Sustainable microbial cell nanofactory for zinc oxide nanoparticles production by zinc-tolerant probiotic Lactobacillus plantarum strain TA4. Microb Cell Factories [Internet]. 2020 [cited 2021 Oct 27];19:10. Available from: https://microbialcellfactories.biomedcentral.com/articles/10.1186/s12934-020-1279-6

52. Costantini PE, Firrincieli A, Fedi S, Parolin C, Viti C, Cappelletti M, et al. Insight into phenotypic and genotypic differences between vaginal Lactobacillus crispatus BC5 and Lactobacillus gasseri BC12 to unravel nutritional and stress factors influencing their metabolic activity. Microb Genomics [Internet]. 2021 [cited 2021 Oct 8];7. Available from: https://www.microbiologyresearch.org/content/journal/mgen/10.1099/mgen.0.000575

53. Ibrahim F, Halttunen T, Tahvonen R, Salminen S. Probiotic bacteria as potential detoxification tools: assessing their heavy metal binding isotherms. Can J Microbiol [Internet]. 2006 [cited 2021 Oct 31];52:877–85. Available from: http://www.nrcresearchpress.com/doi/10.1139/w06-043

54. Halttunen T, Salminen S, Meriluoto J, Tahvonen R, Lertola K. Reversible surface binding of cadmium and lead by lactic acid and bifidobacteria. Int J Food Microbiol [Internet]. 2008 [cited 2021 Oct 31];125:170–5. Available from: https://linkinghub.elsevier.com/retrieve/pii/S0168160508001645

55. Kirillova AV, Danilushkina AA, Irisov DS, Bruslik NL, Fakhrullin RF, Zakharov YA, et al. Assessment of Resistance and Bioremediation Ability of *Lactobacillus* Strains to Lead and Cadmium. Int J Microbiol [Internet]. 2017 [cited 2021 Oct 8];2017:1–7. Available from: https://www.hindawi.com/journals/ijmicro/2017/9869145/

56. Udelhoven T, Naumann D, Schmitt J. Development of a hierarchical classification system with artificial neural networks and FT-IR spectra for the identification of bacteria. Appl Spectrosc [Internet]. OSA; 2000;54:1471–9. Available from: http://as.osa.org/abstract.cfm?URI=as-54-10-1471

57. Winder CL, Goodacre R. Comparison of diffuse-reflectance absorbance and attenuated total reflectance FT-IR for the discrimination of bacteria. The Analyst [Internet]. 2004 [cited 2021 Aug 13];129:1118. Available from: http://xlink.rsc.org/?DOI=b408169b

58. Naumann D. Infrared Spectroscopy in Microbiology. In: Meyers RA, editor. Encycl Anal Chem [Internet]. Chichester, UK: John Wiley & Sons, Ltd; 2006 [cited 2020 Mar 29]. p. a0117. Available from: http://doi.wiley.com/10.1002/9780470027318.a0117

59. AlRabiah H, Correa E, Upton M, Goodacre R. High-throughput phenotyping of uropathogenic *E. coli* isolates with Fourier transform infrared spectroscopy. The Analyst [Internet]. 2013 [cited 2021 Aug 13];138:1363. Available from: http://xlink.rsc.org/?DOI=c3an36517d

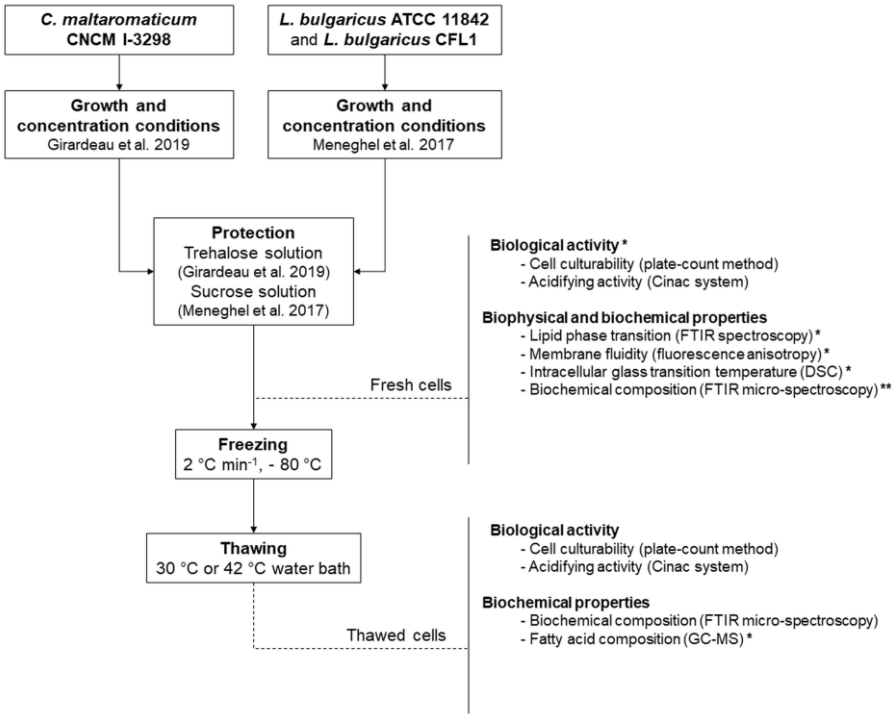

Fig.1 Diagram of the experimental approach used in this study and the main investigated parameters. The asterisks (*) and (**) indicate that the corresponding results for *L. bulgaricus* ATCC 11842 and *L. bulgaricus* CFL1 cells were taken from Meneghel et al. [2] and Meneghel et al. [33], respectively.

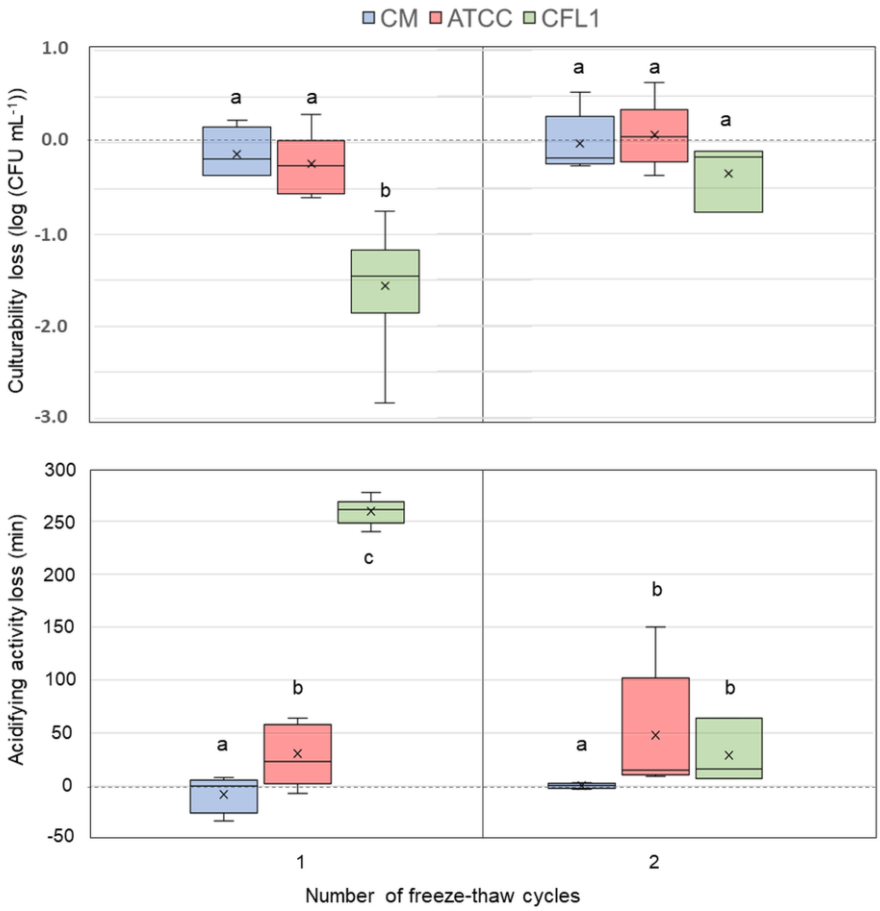

Fig.2 Biological activity loss (culturability loss determined by plate counts method and acidifying activity loss determined with the Cinac system, median values) of *C. maltaromaticum* CNCM I-3298 (CM), *L. bulgaricus* ATCC 11842 (ATCC) and *L. bulgaricus* CFL1 (CFL1) cells following two freeze-thaw cycles. Letters (a, b, c) represent statistical differences between samples at a 95 % confidence level.

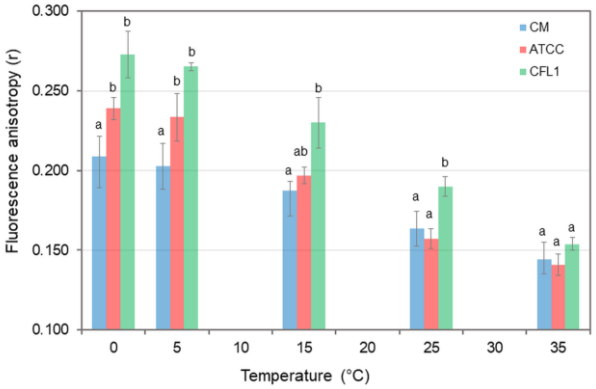

Fig.3 Membrane fluorescence anisotropy (median values) upon cooling of *C. maltaromaticum* CNCM I-3298 (CM, blue bars), *L. bulgaricus* ATCC 11842 (ATCC, red bars) and *L. bulgaricus* CFL1 (CFL1, green bars) cells suspended in a 25 % sucrose solution. Bars correspond to the medians of at least three replicates for each strain at each temperature and the error bars to the associated interquartile ranges. Letters (a, b) represent statistical differences between samples at each temperature at a 95 % confidence level.

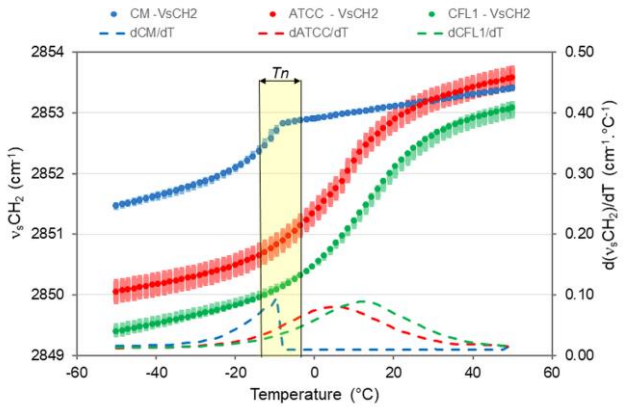

Fig.4 Peak positions of the symmetric CH_2 stretching vibration band (ν_sCH_2) arising from *C. maltaromaticum* CNCM I-3298 (CM, blue circles), *L. bulgaricus* ATCC 11842 (ATCC, red circles) and *L. bulgaricus* CFl1 (CFL1, green circles) upon cooling of fresh cells suspended in a 25 % sucrose solution. Data points correspond to the medians of three replicates for each strain and the error bars to the associated interquartile ranges. The temperature range of water nucleation (Tn) is highlighted. Dotted curves indicate the first derivatives of the symmetric CH_2 stretching vibration band (ν_sCH_2), and the maximum of each curve corresponds to the lipid transition temperature Ts reported in Table 2 for each microorganism.

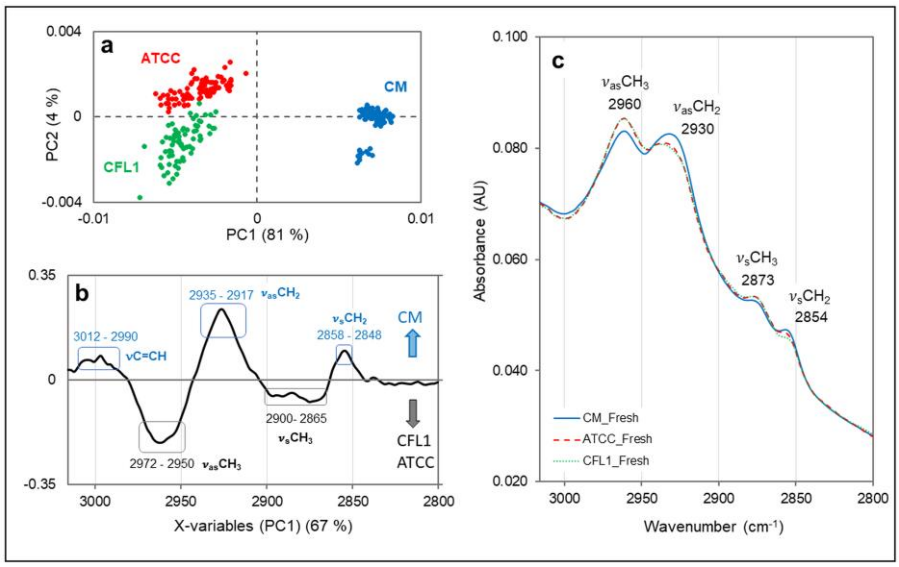

Fig.5 Principal component analysis (PCA) of FTIR baseline-corrected and normalized spectra of fresh *C. maltaromaticum* CNCM I-3298 (CM, blue circles), *L. bulgaricus* ATCC 11842 (ATCC, red circles) and *L. bulgaricus* CFL1 (CFL1, green circles) cells in an aqueous environment, in the 3016 cm^{-1} to 2800 cm^{-1} range: **a** PC1 versus PC2 score plots explaining 81 % and 4 % of the variance, respectively. **b** Loading plot of PC1, separating CM from ATCC and CFL1: positive peaks in PC1 characterized *C. maltaromaticum* , whereas negative peaks characterized *L. bulgaricus* ATCC and CFL1 cells **c** Mean FTIR spectra of fresh cells used for the PCA. The characteristic absorption bands arising from fatty acid chains are indicated.

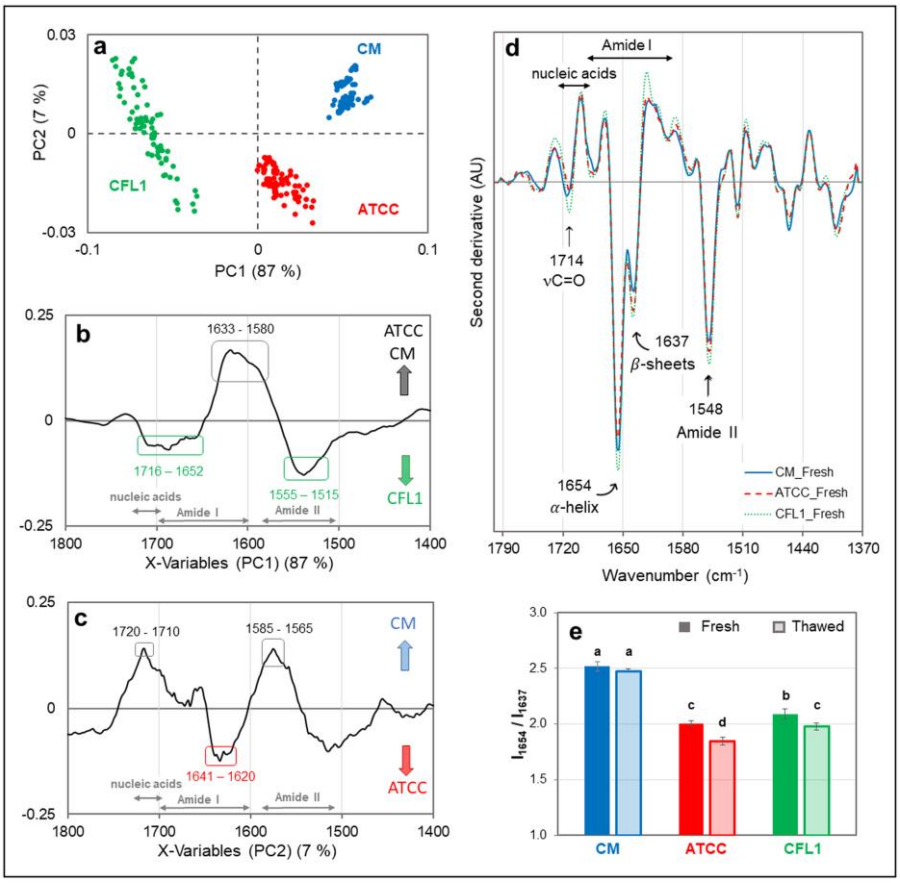

Fig.6 Principal component analysis (PCA) of FTIR baseline-corrected and normalized spectra of fresh *C. maltaromaticum* (CM, blue circles), *L. bulgaricus* ATCC 11842 (ATCC, red circles) and *L. bulgaricus* CFL1 (CFL1, green circles) cells in an aqueous environment, in the 1800 cm^{-1} to 1370 cm^{-1} range: **a** PC1 versus PC2 score plots explaining 87 % and 7 % of the variance, respectively. **b, c** Loading plots of the PC1 and PC2 axis, respectively. Positive peaks in PC1 characterized *C. maltaromaticum* and *L. bulgaricus* ATCC 11842 cells, whereas negative peaks characterized *L. bulgaricus* CFL1 cells. Positive peaks in PC2 characterized *C. maltaromaticum* cells, whereas negative peaks characterized *L. bulgaricus* ATCC 11842. **d** Mean second derivatives of the FTIR spectra of fresh cells used for the PCA. The characteristic absorption bands arising from esters and nucleic acids, protein secondary structures (α-helix, β-sheets) and Amide II are indicated. **e** Mean ratios of the α-helix and β-sheets band intensities at respectively 1654 cm^{-1} and 1637 cm^{-1} of the derived spectra measured in fresh (dark bars) and thawed (light bars) cells**.** Letters (a, b, c, d) represent statistical differences between samples at a 95 % confidence level.

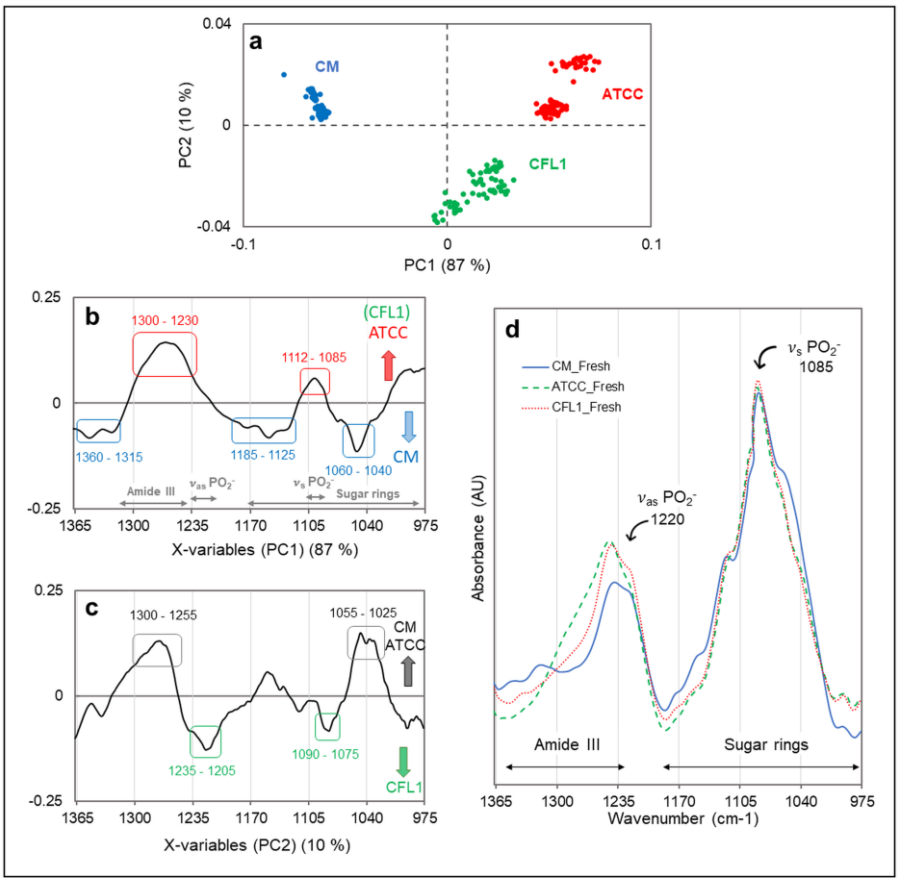

Fig.7 Principal component analysis (PCA) of FTIR baseline-corrected and normalized spectra of fresh *C. maltaromaticum* CNCM I-3298 (CM, blue circles), *L. bulgaricus* ATCC 11842 (ATCC, red circles) and *L. bulgaricus* CFL1 (CFL1, green circles) cells in an aqueous environment, in the 1367 cm^{-1} to 975 cm^{-1} range: **a** PC1 versus PC2 score plots explaining 87 % and 10 % of variance, respectively. **b, c** Loading plots of the PC1 and PC2 axis, respectively. Positive peaks in PC1 characterized *L. bulgaricus* ATCC 11842 and CFL1 cells, whereas negative peaks characterized *C. maltaromaticum* cells. Positive peaks in PC2 characterized *C. maltaromaticum* and *L. bulgaricus* ATCC 11842 and CFL1 cells, whereas negative peaks characterized *L. bulgaricus* CFL1 cells. **d** Mean FTIR spectra of fresh cells used for the PCA. The Amide III region and the characteristic absorption bands of PO_2^- , as well as the sugar rings region are indicated**.**

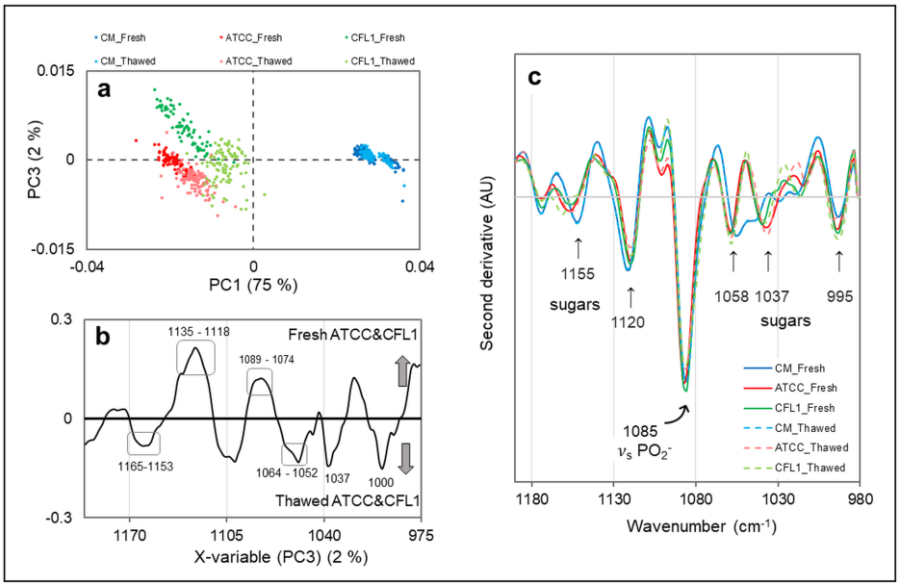

Fig.8 Principal component analysis (PCA) of FTIR baseline-corrected and normalized spectra of fresh and thawed *C. maltaromaticum* CNCM I-3298 (CM, blue circles), *L. bulgaricus* ATCC 11842 (ATCC, red circles) and *L. bulgaricus* CFL1 (CFL1, green circles) cells in an aqueous environment, in the 1200 cm^{-1} to 975 cm^{-1} range: **a** PC1 versus PC3 score plot explaining 75 % and 2 % of variance, respectively. **b** loading plot of PC3, indicating separation of *L. bulgaricus* ATCC 11842 and *L. bulgaricus* CFL1 thawed cells from fresh cells, shifting to negative values of PC3 after freeze-thawing. **c** Mean second derivatives of the FTIR spectra of fresh and thawed cells used for the PCA. The characteristic symmetric absorption band of PO_2^- and sugar rings are indicated**.**

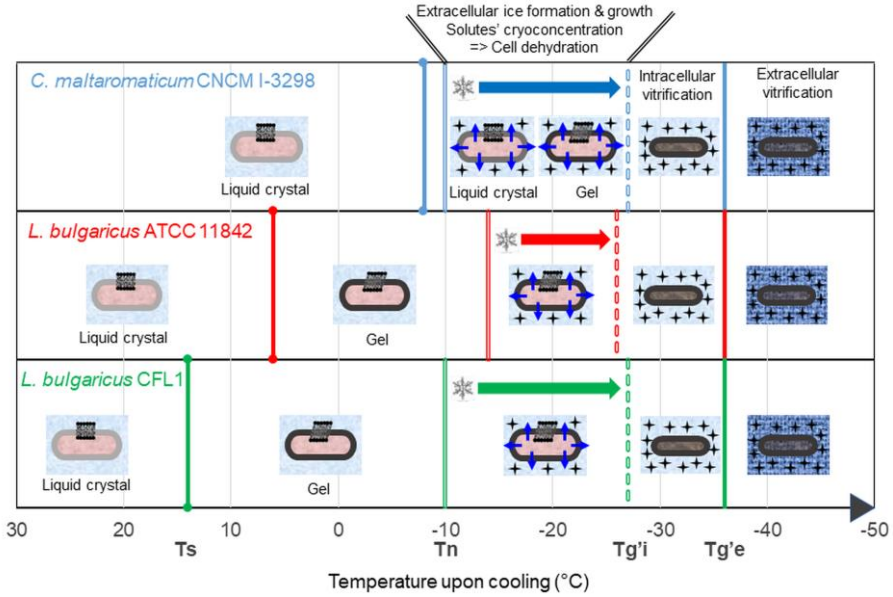

Fig.9 Schematic representation of the behavior of the three LAB cells following freezing from the culture temperature to -80°C, considering the major physical events taking place: membrane lipid phase transition at Ts, ice nucleation at Tn, intracellular glass transition of cryoprotected cells at Tg'i and glass transition of the extracellular medium (20 % sucrose in saline water) at Tg'e.

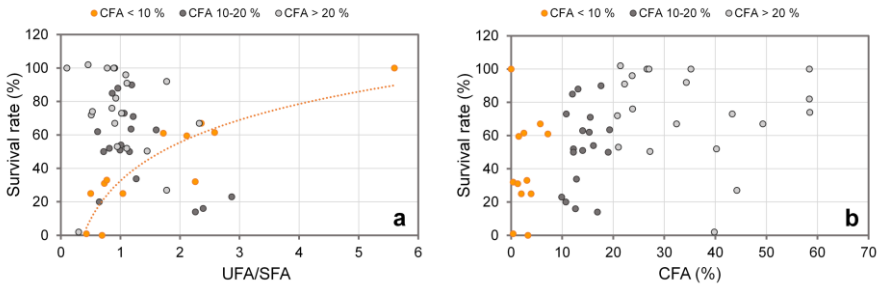

Fig.10 Effect of the membrane fatty acid composition on the survival rate of LAB after freezing, according to the literature [2,3,5,13–17,20,22]. The survival rate is presented as a function of (**a**) the ratio (UFA/SFA) between the unsaturated fatty acids (UFA) and the saturated fatty acids (SFA) and (**b**) the cyclic fatty acid (CFA) content expressed as a percentage of total membrane fatty acids. The data is grouped according to the CFA content: CFA lower than 10 % (orange circles), CFA values between 10 and 20 % (dark grey circles), and CFA values higher than 20 % (light grey circles).